A cellular dynamical mean field theory approach to Mottness

Tudor D. Stanescu [*], Marcello Civelli [1], Kristjan Haule, Gabriel Kotliar

Center for Materials Theory, Department of Physics and Astronomy, Rutgers University, Piscataway, NJ 08854-8019, USA

Received 27 February 2006; accepted 31 March 2006

Abstract

We investigate the properties of a strongly correlated electron system in the proximity of a Mott insulating phase within the Hubbard model, using a cluster generalization of the dynamical mean field theory. We find that Mottness is intimately connected with the existence in momentum space of a surface of zeros of the single particle Green's function. The opening of a Mott–Hubbard gap at half filling and the opening of a pseudogap at finite doping are necessary elements for the existence of this surface. At the same time, the Fermi surface may change topology or even disappear. Within this framework, we provide a simple picture for the appearance of Fermi arcs. We identify the strong short-range correlations as the source of these phenomena and we identify the cumulant as the natural irreducible quantity capable of describing this short-range physics. We develop a new version of the cellular dynamical mean field theory based on cumulants that provides the tools for a unified treatment of general lattice Hamiltonians.
© 2006 Elsevier Inc. All rights reserved.

1. Introduction

The role played by strong correlations in interacting many-particle systems was brought into spotlight half a century ago by Sir Neville Mott [1] in the context of metal–insulator

---

[*] Corresponding author. Present address: Department of Physics, University of Virginia, Charlottesville, VA 22904-4714, USA. Fax: +1 434 924 4576.
  E-mail address: ts2eg@virginia.edu (T.D. Stanescu).
[1] Present address: Institut Laue Langevin, 6 Rue Jules Horowitz, 38042 Grenoble Cedex, France.

transitions. In the last decades, the interest in the field of strongly correlated electrons has increased tremendously, fueled by the discovery of heavy fermion compounds, organic conductors, and high temperature superconductors. Yet, in spite of many advances on both the experimental and theoretical fronts, understanding the physics of these materials continues to represent one of the most difficult open problems in condensed matter physics. The difficulties faced by the theoretical studies stem from the fact that in these systems the inter-particle interactions are comparable or larger than the kinetic energy. Consequently, it is at least questionable to proceed along the conventional paths of many-body physics, starting from a perturbative expansion around the non-interacting limit. The situation is clearly illustrated by the parent materials of cuprate superconductors, composed of CuO_2 planes separated by spacer layers. As the number of electrons per copper site is odd, band theory predicts that these materials are metals, but in reality they are insulators characterized by a sizable energy gap. The source of the insulating behavior consists of correlation effects. The essence of these effects can be captured by simple models, such as the Hubbard model [2]. While solving such a model represents a real theoretical challenge, the solutions of these simply looking problems are crucial for understanding strong correlations. In addition to the Mott–Hubbard gap, strong correlations are responsible for other anomalous phenomena, such as the occurrence of a pseudogap, or the spectral weight transfer over large energy scales. We refer to these key features that characterize the physics of strongly correlated systems by the term Mottness. This constitutes the background for a plethora of ordered phases such as anti-ferromagnetism, charge ordering, or superconductivity.

A significant step forward in the study of strongly correlated systems was made through the development of dynamical mean field theory (DMFT) [3–6] (for a review see Ref. [7]). Within DMFT, the infinite number of degrees of freedom associated with the interacting lattice problem is separated into two sets. A small number of degrees of freedom, namely those responsible for the local correlations, are treated explicitly, while the rest are considered as mean-fields acting on the first set. In the limit of infinite dimensions, the self-energy of the many-body Green's function becomes local. Based on this property, DMFT maps the interacting lattice problem onto an Anderson impurity problem with an effective bath that is determined self-consistently. While the mapping is exact only for $d = \infty$, single-site DMFT represents an excellent approximation for finite dimensional systems whenever the essential aspects of the physics of a given material are local. For example, DMFT was very successful in providing a unified framework for understanding the physics of the finite temperature Mott transition in materials such as V_2O_3, answering some of the most long-standing open questions in strongly correlated electron systems.

Despite its great success, single-site DMFT has limitations that stem from neglecting non-local quantum fluctuations. As a consequence, the theory cannot describe phases characterized by non-local order parameters, such as d-wave superconductivity. Even the existence of a normal state pseudogap in model Hamiltonians, which would correspond to the phenomenon observed in underdoped cuprates, is in contrast with the DMFT prediction of a Fermi liquid at any non-zero doping value. To address these limitations, several cluster extensions of the single-site DMFT that incorporate short-range correlations explicitly have been proposed [8–12]. The great advantage of DMFT and of its cluster generalizations consists in being non-perturbative approaches that are always in the thermodynamic limit. In addition, these approximations can be systematically improved by increasing the size of the effective impurity problem. Using this methodology one

can identify the minimal cluster size required to describe certain phenomena. As this minimal size is related to the range of relevant correlations, the method offers further insight into the physics of the problem. Studies using small cluster sizes, $N_c = 2$ or $N_c = 4$, have already opened new perspectives in understanding the Hubbard or the t–J models and have unveiled many aspects that are relevant to the physics of the cuprates, such as the Mott–Hubbard transition in two dimensions [13–16], the generation of the pseudogap [17–19], the momentum space dependence of the spectral function [15,20,21], or the basic elements of the phase diagram [8,12,22].

Unlike single-site DMFT, the cluster extensions are not unique. The dynamical cluster approximation (DCA) [8], for example, is naturally defined in momentum space. The corresponding real space cluster has periodic boundary conditions that preserve explicitly the translational symmetries of the lattice. In contrast, the cellular dynamical mean field theory (CDMFT) [10] represents a direct generalization of DMFT to a real space cluster having open boundary conditions. The cluster solution violates the translational symmetry of the lattice which is restored in a second step, after the effective cluster problem has been solved, by properly re-constructing the lattice quantities from their cluster counterparts. While in the limit of large clusters the solutions obtained with the two methods are identical, finite size approximations may differ, especially for small clusters, and special care is required in interpreting the results. Also, the difference in boundary conditions is reflected in a different asymptotic behavior. For a large linear cluster of size N_c DCA converges like $\mathcal{O}(1/N_c^2)$, while the CDMFT solution, due to the fact that the effective bath couples only with the boundary sites, is characterized by a surface region with a slow $\mathcal{O}(1/N_c)$ convergence and a bulk region where the solution converges exponentially. Therefore, depending on the nature of the problem considered, one approach or the other may be more suitable.

In the present article we address one of the key aspects underlying any cluster DMFT approach to Mottness: does the implicit assumption that the self-energy is a short-range quantity hold? If not, what are the implications for the cluster DMFT techniques themselves and for our understanding of Mottness? In a recent study [23], it was shown that the irreducible two-point cumulant, rather than the self-energy, represents the basic irreducible object that is short-range in or close to a Mott insulating phase. While this finding does not imply a change in the DMFT equations for the Hubbard model, it has consequences for a general lattice problem. More importantly, the correct procedure for re-constructing the lattice quantities has to take into consideration this fact, regardless of the details of the implementation of the cluster method. This observation leads to a new insight into the physics of high temperature superconductors. We find that the origin of the pseudogap state is associated with the formation of lines of zeroes of the single particle Green's function. It is the presence of these lines that determines the opening at the Fermi energy of a momentum dependent pseudogap. In addition, if a zero line lays in the proximity of the Fermi surface, which is the line of poles of the Green's function, the corresponding quasiparticle weights vanish. This effect is responsible for the appearance of Fermi arcs in the single particle spectral function, as detected in ARPES experiments [26,27].

We argue that cluster generalizations of DMFT, for example the cellular dynamical mean field theory (CDMFT), not only represent powerful computational tools for tackling strongly correlated many-body problems, but are able to reveal some of the deep physical aspects of Mottness. On the methodological side, we identify the ingredients necessary in

order to incorporate in the cluster schemes the fact that the cumulant, not the self-energy, is the natural short-range irreducible quantity that has to be used, and we formulate explicitly a Cellular DMFT approach based on cumulants. Using this approach we find that in the vicinity of the Mott insulating phase a system is characterized by the presence of zeros in the zero frequency Green's function at zero temperature. The presence of the zero lines produces the opening at the Fermi energy of a momentum dependent pseudogap in the single particle spectral function. In addition, if a zero line lays in the proximity of the Fermi surface, which is the line of infinities of the Green's function, the corresponding quasiparticle weights vanish. This effect is responsible for the apparition of Fermi arcs in the single particle spectral function.

The article is organized as follows: in Section 2, we provide the details of the cluster approach. We construct a generalization of the cellular dynamical mean field theory having cumulants as the main irreducible quantities. We emphasize the importance of the lattice re-construction step in a cluster DMFT scheme and discuss the underlying physics. In Section 3, we present a series of results that illustrate the behavior of the cluster quantities for systems close to the Mott insulating phase, in particular the emergence of a pseudogap in the single particle spectral function. Section 4 consists of two parts. In the first part we establish that, in the presence of Mottness, the self-energy is a long range quantity that cannot be described properly within a small cluster calculation. In contrast, the cumulant is short range and, even within small cluster approximations, reproduces correctly the main features of the system. The implications of this finding for the low energy physics of a correlated metal are discussed in the second part of Section 4. Finally, our conclusions and some open questions are presented in Section 5.

2. Cellular dynamical mean field theory: the strong coupling picture

In this Section, we outline a strong coupling approach [28] that represents the natural framework for a generalization of DMFT. The formalism can be applied to any lattice problem, providing the tools for a unified treatment of any non-local contribution to the Hamiltonian. For example, the treatment of correlated hopping [29,30], and the extended DMFT [32–36] are limiting cases of this unified approach. Within this scheme, non-local terms such as hopping terms, spin–spin interactions, or non-local Coulomb interactions are treated on equal footing. Most importantly, this method introduces as basic building block the irreducible cumulant, instead of the self-energy, identifying it as the short-range quantity necessary for the study of Mottness.

Using the notation of Ref. [28], we start with a general lattice Hamiltonian

$$H = H_0 + H_1, \tag{1}$$

containing a local term, H_0, and a non-local term, H_1 that can be expressed using Hubbard operators, $X_i^{\alpha\beta}$, as

$$H_0 = \sum_i \sum_\alpha \lambda_\alpha X_i^{\alpha\alpha}, \tag{2}$$

and

$$H_1 = \sum_{i \neq j} \sum_{\alpha,\beta,\alpha',\beta'} E_{ij}^{\alpha\beta\alpha'\beta'} X_i^{\alpha\beta} X_j^{\alpha'\beta'}. \tag{3}$$

In Eqs. (2) and (3) α, β, α' and β' represent single-site states which, taking for simplicity the case of spin $\frac{1}{2}$ fermions, are: $|0\rangle$ (empty site), $|\uparrow\rangle$ (single occupied site with spin up), $|\downarrow\rangle$ (single occupied site, spin down), and $|2\rangle$ (double occupied site). The Hubbard operators $X_i^{\alpha\beta}$ describe transitions between these states and have a fermionic character if the occupation numbers of the states α and β differ by one, and bosonic character otherwise. The parameters λ_α in Eq. (2) represent the single-site energies and are determined by the chemical potential μ, the on-site Hubbard interaction U, and the external fields. The coupling constants $E_{ij}^{\alpha\beta\alpha'\beta'}$ may include contributions coming for example from hopping t_{ij}, spin–spin interaction J_{ij}, or non-local Coulomb interaction V_{ij}. Within the present approach, all these contributions are treated on equal footing, and we can regard $E_{ij}^{\alpha\beta\alpha'\beta'}$ as generalized "hopping" matrix elements. To simplify the notations, in this article we will use a single Greek letter, for example μ or v, for pairs of single site states (α, β). Also, we will use the notations $\mathbf{A}$, for a matrix with elements $A^{\mu v} = A^{\alpha\beta\alpha'\beta'}$, and $\hat{\mathbf{A}}$ for a tensor $A_{ij}^{\mu v}$.

The main object that we want to determine is the Green's function of the Hubbard operators. However, the theory is expressed naturally in terms of a generalized irreducible two-point cumulant, M. We define the Green's function as

$$G_{ij}^{\mu v}(\tau, \tau') = -\mathrm{Tr}\{\hat{\rho}\hat{T}[X_i^\mu(\tau)X_j^v(\tau')]\} + \langle X_i^\mu\rangle\langle X_j^v\rangle, \tag{4}$$

where the Hubbard operators are in the Heisenberg representation,

$$X_i^{\alpha\beta}(\tau) = \mathrm{e}^{H\tau}X_i^{\alpha\beta}\mathrm{e}^{-H\tau} \tag{5}$$

and the statistical operator is

$$\hat{\rho} \equiv \mathrm{e}^{-\beta H_0}\hat{\sigma}(\beta) = \mathrm{e}^{-\beta H_0}\hat{T}\exp\left\{-\int_0^\beta \mathrm{d}\tau H_1(\tau)\right\}. \tag{6}$$

The formal relationship between the Green's function and the two-point irreducible cumulant can be obtained by performing a re-summation of the strong coupling expansion in the generalized hopping [28]. Diagrammatically, the irreducible cumulant is defined as the sum of all connected diagrams having two external legs with the property that the two legs cannot be separated by cutting one hopping line. Notice that the definition differs slightly from the standard definition [37,7], which requires that the diagram be not disconnected by cutting a single line. This is due to the presence of cumulants with odd number of legs generated by bosonic X-operators with a non-zero average $\langle X\rangle$ (see Ref. [28]). Explicitly, we have

$$G_{ij}^{\mu v} = M_{ij}^{\mu v} + \sum_{k,l}\sum_{\rho,\pi} M_{ik}^{\mu\rho}E_{kl}^{\rho\pi}G_{lj}^{\pi v}, \tag{7}$$

and, for a translation invariant system

$$\mathbf{G}(\mathbf{k}, \mathrm{i}\omega_n) = [\mathbf{M}^{-1}(\mathbf{k}, \mathrm{i}\omega_n) - \mathbf{E}(\mathbf{k})]^{-1}, \tag{8}$$

where $\mathbf{E}(\mathbf{k})$ is the Fourier transform of the coupling constant matrix.

The approximations that define a DMFT-type scheme can be introduced in an elegant way by constructing functionals of the quantities of interest, such as Green's functions or self-energies. In this framework one can derive the original, single site DMFT equations [7], the extended DMFT equations [36], and other similar schemes [11]. In principle, these functionals can be constructed order by order in a perturbative

expansion in the interactions. Systematic approximations can be obtained, for example, by restricting the argument of the Baym–Kadanoff functional $\Phi[G]$ from the full Green's function to a Green's function defined only inside a cluster of sites and its periodic supercell repetition. The standard derivations use a weak-coupling framework in which the Green's function and the self-energy represent a pair of "conjugate" quantities and the Baym–Kadanoff functional is defined as the sum of all vacuum-to-vacuum skeleton (two-particle irreducible) diagrams constructed with the full propagator G and the interaction vertex. A complementary strong coupling picture can be obtained by constructing the functionals starting from a perturbative expansion in hoping [30,28]. Within this picture, the basic quantities are the irreducible cumulant and its conjugate, the renormalized coupling constant (or renormalized generalized hopping), $\hat{\mathcal{E}}$, instead of the self-energy and the Green's function, respectively. The quantity $\hat{\mathcal{E}}$ can be represented diagrammatically as a sum of chains of "hopping" lines and irreducible cumulants. Analytically we have

$$\mathcal{E}_{ij}^{\mu\nu} = E_{ij}^{\mu\nu} + \sum_{p,q} \sum_{\alpha,\beta} E_{iq}^{\mu\alpha} M_{qp}^{\alpha\beta} E_{pj}^{\beta\nu} + \cdots = [\hat{\mathbf{E}}(\hat{\mathbf{I}} - \hat{\mathbf{M}}\hat{\mathbf{E}})^{-1}]_{ij}^{\mu\nu}, \tag{9}$$

where $\hat{\mathbf{I}}$ represents the unit tensor. In addition, the strong coupling functional depends on the average $Q_i = \langle X_i \rangle$ of the bosonic Hubbard operators which can be interpreted as a generalized "magnetization". Its conjugate, h_i, represents a generalized "magnetic" field. Typically, these quantities are non-zero if the system is in a broken symmetry phase and zero otherwise. Explicitly, the strong coupling functional is [28]

$$\Gamma[\mathcal{E}, Q] = \Omega_0 + \frac{1}{\beta} \sum_{\omega_n} \mathrm{Tr} \ln[\hat{\mathbf{I}} - \hat{\mathbf{M}}[\mathcal{E}, Q]\hat{\mathbf{E}}] + \frac{1}{\beta} \sum_{\omega_n} \mathrm{Tr}[\hat{\mathbf{M}}[\mathcal{E}, Q]\hat{\mathcal{E}}]$$
$$- \frac{1}{2} \sum_{i,j} \sum_{\mu,\nu} Q_i^\mu E_{ij}^{\mu\nu} Q_j^\nu + \Psi[\mathcal{E}, Q], \tag{10}$$

where β represents the inverse temperature and $\Psi[\mathcal{E}, Q]$ is the strong coupling equivalent of the Baym–Kadanoff functional and can be represented diagrammatically as a sum over all the skeleton diagrams that are two-particle irreducible with respect to the renormalized hopping lines $\mathcal{E}$ and contain bare cumulants nodes dressed with EQ contributions. The stationarity condition $\delta\Gamma/\delta\mathcal{E}_{ji}^{\nu\mu} = 0$ yields

$$-\beta \frac{\delta\Psi[\mathcal{E}, Q]}{\delta\mathcal{E}_{ji}^{\nu\mu}(\mathrm{i}\omega_n)} = M_{ij}^{\mu\nu}(\mathrm{i}\omega_n). \tag{11}$$

In addition, stationarity with respect to Q, $\delta\Gamma/\delta Q_i^\mu = 0$, determines the generalized "magnetic" fields

$$h_i^\mu \equiv \frac{\delta\Psi[\mathcal{E}, Q]}{\delta Q_i^\mu} = \sum_{j,\beta\in\mathcal{B}_Q} E_{ij}^{\mu\nu} Q_j^\nu. \tag{12}$$

A cluster DMFT scheme consists of two major steps: (1) a recipe for mapping the full lattice problem onto an effective cluster problem, and (2) a recipe for re-constructing the lattice quantities from their cluster counterparts. The effective quantum impurity problem can be solved using, for example, perturbative approaches, such as NCA, or numerical methods, such as Quantum Monte Carlo (QMC), or exact diagonalization (ED). The

use of these "impurity solvers" is independent of the cluster scheme, defined uniquely by the two steps described above, and may be dictated by the range of parameters of interest (for example temperature, strength of the interaction, or size of the cluster) or the available computer power. Within the CDMFT approach we start by constructing a super-lattice by tiling the original lattice with identical clusters containing N_c sites. The cells of this super-lattice are treated as "single" sites with internal degrees of freedom. Using the strong coupling functional approach, the CDMFT scheme is introduced by restricting the argument of the Baym–Kadanoff functional Ψ from the full renormalized hopping to a function $\mathcal{E}_{ij}$ defined only inside the cells of the super-lattice:

$$\Psi^{(\mathrm{SL})}[\mathcal{E}, Q] = \sum_c \psi[\mathcal{E}_{i_c j_c}, Q], \tag{13}$$

where 'c' represents a certain cell and $(i_c j_c)$ a pair of sites inside the cell 'c'. A direct consequence of this ansatz is that the two-point irreducible cumulant of the theory is short-ranged,

$$\mathbf{M}_{i_{c_1} j_{c_2}}(\mathrm{i}\omega_n) = \frac{\delta \Psi}{\delta \mathcal{E}_{i_{c_1} i_{c_1}}(\mathrm{i}\omega_n)} \delta_{c_1 c_2}, \tag{14}$$

with δ_{ij} being the Kronecker δ symbol. If the distance $|\mathbf{R}_{i_{c_1}} - \mathbf{R}_{i_{c_2}}|$ is larger than the size of the cluster, c_1 and c_2 represent necessarily different cells and, consequently, the cumulant vanishes. To complete the fist step of the construction let us observe that the functional $\psi[\mathcal{E}_{i_c j_c}, Q]$ can be determined by solving a quantum impurity problem with N_c impurities coupled to an infinite non-interacting bath. The impurity problem is defined on a real space cluster $\mathcal{C}$ by the statistical operator

$$\hat{\rho}_{\mathrm{imp}} = \mathrm{e}^{-\beta H_0^{\mathrm{imp}}} \hat{T} \exp \left\{ - \int_0^\beta \mathrm{d}\tau \left[\int_0^\beta \mathrm{d}\tau' \sum_{\mu,\nu} \sum_{i,j} X_i^\mu(\tau) [\mathit{\Delta}_{ij}^{\mu\nu}(\tau - \tau') + \delta(\tau - \tau') E_{ij}^{\mu\nu}] X_j^\nu(\tau') \right. \right.$$
$$\left. \left. + \sum_{i,\mu} h_i^\mu(\tau) X_i^\mu(\tau) \right] \right\}, \tag{15}$$

where $h(\tau)$ is an external field that couples to the bosonic X-operators, $\mathbf{\Delta}(\tau - \tau')$ is the hybridization matrix and $H_0^{\mathrm{imp}} = \sum_{i \in \mathcal{C}} \sum_\alpha \lambda_i X_i^{\alpha\alpha}$ is the local cluster Hamiltonian. The functional construction described above for the lattice problem can also be implemented for the cluster impurity problem. The corresponding strong coupling impurity functional is

$$\Gamma_{\mathrm{imp}}[\mathcal{D}, Q] = \frac{\Omega_0}{N} + \frac{1}{\beta} \sum_{\omega_n} \mathrm{Tr} \ln[\hat{\mathbf{I}} - \hat{\mathbf{M}}_{\mathrm{imp}}[\mathcal{D}, Q] \hat{\mathbf{D}}] + \frac{1}{\beta} \sum_{\omega_n} \mathrm{Tr}[\hat{\mathbf{M}}_{\mathrm{imp}}[\mathcal{D}, Q] \hat{\mathcal{D}}]$$
$$- \frac{1}{2} \sum_{i,j} \sum_{\mu,\nu} Q_i^\mu [E_{ij}^{\mu\nu} + \mathit{\Delta}_{ij}^{\mu\nu}(0)] Q_j^\nu - \sum_{\mu,i \in \mathcal{C}} h_i^\mu Q_i^\mu + \Psi_{\mathrm{imp}}[\mathcal{D}, Q], \tag{16}$$

where $\mathcal{D} = \mathbf{\Delta}[\mathbf{I} - \mathbf{M}_{\mathrm{imp}} \mathbf{\Delta}]^{-1}$ is the renormalized hybridization tensor, $Q_i^\mu = \langle X_i^\mu \rangle$ and $\mathit{\Delta}_{ij}^{\mu\nu}(0)$ is the hybridization at zero frequency. In addition, the impurity problem contains the effective fields h_i^μ that couple with the non-zero average Q_i^μ of bosonic Hubbard operators. The diagrammatic representation of the generalized Luttinger-Ward potential $\Psi_{\mathrm{imp}}[\mathcal{D}, Q]$ is identical with that of its lattice correspondent and we have $\psi = \Psi_{\mathrm{imp}}$, i.e. the two functionals coincide, provided:

$$\mathcal{E}_{ij}^{\mu\nu} = \mathcal{D}_{ij}^{\mu\nu} \quad \text{for any } i, j \in \mathcal{C}, \tag{17}$$

$$\sum_{p\notin\mathcal{C}} \sum_{\nu} E_{ip}^{\mu\nu} \langle X_p^{\nu} \rangle = h_i^{\mu} + \sum_{j\in\mathcal{C}} \sum_{\nu} \Delta_{ij}^{\mu\nu}(0) \langle X_j^{\nu} \rangle. \tag{18}$$

These relations determine the Weiss fields $\Delta_{ij}^{\mu\nu}$ and h_i^{μ} and define the self-consistent mapping of the super-lattice problem defined by Eq. (13) onto a N_c-impurity problem. Finally, it is convenient to cast Eq. (17) into a more familiar form as an equality between the Green's function matrix for the impurity cluster and the Green's function matrix for one cell of the super-lattice. After a little algebra, Eq. (17) can by re-written as

$$\sum_{\kappa\in RBZ} [\hat{\mathbf{M}}_c^{-1} - \hat{\mathbf{E}}_\kappa]^{-1} = [\hat{\mathbf{M}}_c^{-1} - \hat{\mathbf{\Lambda}} - \hat{\mathbf{E}}]^{-1}, \tag{19}$$

where the κ summation extends over the reduced Brillouin zone associated with the super-lattice. Formally, Eq. (19) is very similar to the standard DMFT self-consistency conditions [7,10]. However, we have to remember that the quantities that appear in (19) are tensors having indices that represent positions inside the cluster as well as single site state labels associated with the Hubbard operators. In the particular case of the Hubbard model, one can easily show [28] that Eq. (19) reduces to the standard CDMFT self-consistency condition.

We turn now to the second stage of the CDMFT scheme: the re-construction of the lattice quantities. The question that we have to answer is how to derive good approximations for the lattice quantities using the cluster quantities obtained by solving the effective impurity model. Within CDMFT, the answer to this question depends on the size of the cluster. The physical reason for this originates in the fact that in the CDMFT approach the effective bath couples only with those sites of the cluster that are within hopping range of the exterior. For example, in the case of nearest neighbor hopping, only the boundary sites are coupled to the bath. Consequently, the sites situated within two or three lattice units from the boundary will be characterized by some "surface" values of the local quantities that are weakly dependent on the cluster size, while the "bulk" quantities converge exponentially [24] to the lattice values. Therefore, for large clusters it is convenient to use exclusively, or to weight more, the bulk quantities, while for small clusters having only surface sites an alternative procedure has to be used. In this article we focus on the re-construction procedure for small clusters, as presently there is no data available for large clusters (i.e. clusters containing bulk sites) in two dimensions.

Our procedure for re-constructing lattice quantities takes into account two conditions: (1) The solution has to preserve the symmetry of the lattice. A lower symmetry may obtain only as a result of a broken symmetry in solutions with long range order, and not due to the super-lattice construction. (2) The lattice solution has to be causal, i.e. the lattice Green's function has to satisfy the condition $\text{Im } G(\omega, \mathbf{k}) \leqslant 0$. In the re-construction step, we eliminate the artificial breaking of the translation symmetry introduced by the super-lattice construction. Notice that, in principle, the super lattice construction can also break the original rotation symmetry of the lattice, as for example in the case of tilling a two dimensional square lattice with two-site clusters (links). Also notice that there is a finite number of equivalent ways of covering the lattice with cells of a certain type. This produces equivalent super-lattices that are related to one another by symmetry operations, $\mathcal{S}$. For example, in the case of a square lattice covered with plaquettes we have $v_{\mathcal{S}} = 4$ distinct realizations of the supper-lattice related to one another by the translation operations

generated by the vectors $(0,0)$ (identity), $(a,0)$, $(0,a)$, and (a,a), where a is the lattice spacing. A natural way to restore the original symmetry and produce reasonable lattice estimates is to consider the average of the relevant super-lattice quantity over its equivalent realizations. Explicitly, for the lattice quantity $W(\mathbf{R}_i - \mathbf{R}_j)$ we have

$$W(\mathbf{R}_i - \mathbf{R}_j) = \frac{1}{v_{\mathcal{S}}} \sum_{\mathcal{S}} W^{(\mathrm{SL})}(\mathcal{S}[\mathbf{R}_i], \mathcal{S}[\mathbf{R}_j]), \tag{20}$$

where $W^{(\mathrm{SL})}$ is the corresponding super-lattice quantity and $\mathcal{S}[\mathbf{R}_i]$ is the new position of the site $\mathbf{R}_i$ after applying the symmetry operation $\mathcal{S}$. Notice that equation (20) represents a super-lattice average, not a cluster average. As a consequence, irreducible quantities such as the self-energy, $\Sigma_{nm}^{(\mathrm{SL})}$, or the cumulant, $M_{nm}^{(\mathrm{SL})}$, vanish if the sites $\mathbf{R}_n$ and $\mathbf{R}_m$ belong to different cells of the super-lattice. The question is what quantity $W^{(\mathrm{SL})}$ periodized using Eq. (20) will produce the best estimate for the lattice W? One possibility is to periodize the Green's function [25]

$$\mathbf{G}(\mathbf{k}, \omega) = \frac{1}{N_c} \sum_{i,j \in \mathcal{C}} [\hat{\mathbf{M}}_c^{-1} - \hat{\mathbf{E}}_\mathbf{k}]_{ij}^{-1} e^{i\mathbf{k}(\mathbf{R}_i - \mathbf{R}_j)}, \tag{21}$$

$\hat{\mathbf{E}}_\mathbf{k}$ being the Fourier transform of the "hopping" on the super-lattice, and N_c the number of sites in a cell. Alternatively, we can first periodize irreducible quantities, in particular the self-energy and the cumulant, and then use them to re-construct the lattice Green's function. In this article we focus on these last two possibilities as their physical meaning is more transparent. Explicitly, the periodization of a particular irreducible quantity W is valid as long as W represents a short-range quantity, so that reasonable approximations for its relevant components can be extracted from the effective impurity problem, while components with a range longer than the cluster size can be neglected. A violation of the validity conditions for the procedure leads either to quantitative errors, if W has indeed a finite range but larger than the size of the cluster used in the calculation, or to qualitatively wrong results, if the irreducible quantity is long-ranged. Consequently, a careful analysis of the range or irreducible quantities should be a mandatory step in any cluster DMFT approach. Taking as an example the plaquette covering of a two dimensional square lattice, we have three independent values for the cluster quantities, for example $\Sigma_0 = \Sigma_{ii}$ for the on-site self-energy, $\Sigma_1 = \Sigma_{ij}$, with i and j nearest neighbors, for the link self-energy, and $\Sigma_2 = \Sigma_{ij}$, with i and j next nearest neighbors, for the diagonal self-energy. The super-lattice self-energy $\Sigma_{ij}^{(\mathrm{SL})}$ will have the corresponding cluster value if i and j are in the same cell and zero otherwise. Taking into account the four equivalent realizations of the super-lattice discussed above and performing the average (20), we obtain for the lattice self-energy the expression

$$\boldsymbol{\Sigma}(\mathbf{k}, \omega) = \boldsymbol{\Sigma}_0(\omega) + \boldsymbol{\Sigma}_1(\omega)\alpha(\mathbf{k}) + \boldsymbol{\Sigma}_2(\omega)\beta(\mathbf{k}), \tag{22}$$

where $\alpha(\mathbf{k}) = \cos(k_x) + \cos(k_y)$ and $\beta(\mathbf{k}) = \cos(k_x)\cos(k_y)$. Similarly, we obtain for the periodized lattice cumulant

$$\mathbf{M}(\mathbf{k}, \omega) = \mathbf{M}_0(\omega) + \mathbf{M}_1(\omega)\alpha(\mathbf{k}) + \mathbf{M}_2(\omega)\beta(\mathbf{k}). \tag{23}$$

Notice that in real space the lattice quantities have a finite range given by the size of the cluster used in the approximation and we have $M_0^{\mathrm{latt}} = M_0$, $M_1^{\mathrm{latt}} = 1/2M_1$, and $M_2^{\mathrm{latt}} = 1/4M_2$ for the lattice cumulant M^{latt}, and similar expressions for the self-energy. Consequently, in this construction the local lattice cumulant is the same as the local cluster

cumulant, while the link and next nearest neighbor cumulants are half and a quarter of their cluster counterparts, respectively. Similar coefficients occur in the self-energy period-ization scheme. These coefficients insure that the imaginary parts of the lattice self-energy and cumulant are negative for an arbitrary value of the momentum, i.e. that the Green's functions constructed from them are causal and satisfy the second requirement of the re-construction step. As we mentioned above, the physical assumption behind using Eq. (22) or Eq. (23) is that the self-energy (or the cumulant) are short-range quantities. A detailed comparison between results obtained using these constructions is presented bellow. In the standard implementations of the cluster DMFT schemes the first assumption, i.e. the locality of Σ, was considered. In Section 4 of this article we will show that this assumption fails when Mottness is present and the locality of cumulants has to be considered instead. Moreover, Mottness is associated with a long range self-energy that diverges in certain points of the Brillouin zone producing zeros of the Green's function and therefore the use of cumulants is crucial. Our finding does not apply to CDMFT schemes only, but also to momentum space schemes such as the dynamical cluster approximation (DCA). In this case, any attempt to smoothly interpolate between different patches in the Brillouin zone will have to take into account that the smoothly varying function in k-space is the cumulant, not the self-energy.

3. Cluster quantities and the short-range correlations induced pseudogap

One of the most remarkable features of the normal state of the high-temperature super-conductors is the suppression of the density of states at the Fermi energy. Understanding this pseudogap behavior may be one of the keys in understanding the superconducting mechanism itself. The existence of a pseudogap in the cluster solution of the two-dimen-sional Hubbard model has been obtained by several groups [17–19] using cluster DMFT-type methods. This effect is the result of short-range correlations and no long range order or preformed pairs need to be invoked. In this section we show that this feature occurs naturally in a cluster DMFT scheme as a result of taking into consideration the short-range correlations. The suppression of the density of states at the Fermi level can be seen directly in the cluster solution, in particular in the local cluster spectral function $A_{ii}(\omega) = -1/\pi \, \text{Im} \, G_{ii}(\omega)$. We will also point out some of the properties of this pseudogap, such as the dependence on temperature, doping and strength of the interaction. All the results are obtained using CDMFT with NCA as an impurity solver (for details of the implementation see Ref. [38]). In the next Section we analyze in more detail the nature of the pseudogap, its origin and the connection with the apparition of Fermi arcs.

We start with a half-filled two-dimensional Hubbard model with the on-site interaction $U = 5t$, where t is the hopping matrix element. Throughout this article we use t as the unit for energy. Shown in Fig. 1 is the local spectral function A_{ii} obtained within a CDMFT scheme using a two-site cluster ($N_c = 2$-link) with NCA solver for a temperature $T = 0.2t$. The pseudogap that opens at the Fermi energy, i.e. at $\omega = 0$, separating the lower and upper Hubbard bands represents the finite temperature remnant of the Mott–Hub-bard gap. At any finite temperature we observe a residual non-vanishing zero frequency density of states which increases with temperature. The opening of this gap for small val-ues of the on-site interaction is in sharp contrast with the results of single-site DMFT calculations showing a sharp Kondo-like resonance at the Fermi level [7] and reveals the importance of treating explicitly the short-range correlations. We notice that the
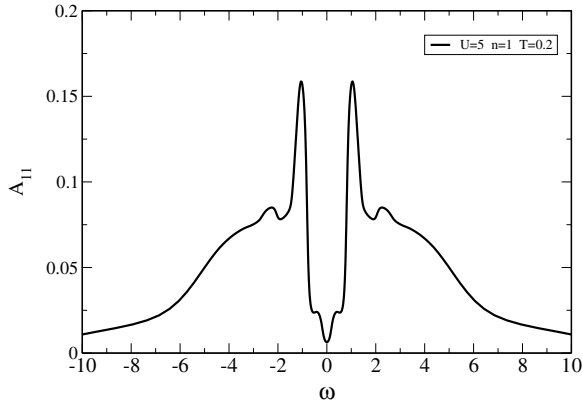
Fig. 1. Cluster density of states for a half-filled two-dimensional Hubbard model using a two site cluster (link) CDMFT with NCA solver.

pseudogap was obtained in the absence of long range antiferromagnetic order by imposing a paramagnetic solution for the DMFT equations. In the case of the half-filled two-dimensional Hubbard model with particle-hole symmetry, i.e. with $t' = 0$, this behavior is observed for any non-zero value of the interaction U suggesting the absence of any finite U metal to insulator transition. This result was confirmed within several cluster DMFT schemes using either NCA [14] or QMC [13,15] impurity solvers, while a recent study [19] using exact diagonalization as an impurity solver seem to suggest otherwise. Finally, let us notice that the two Hubbard bands are characterized by the presence of two narrow sub-bands near the edge of the Mott gap. These additional features become sharper as we lower the temperature simultaneously with an increase of the occupation number of the singlet state in the cluster [31,38]. This behavior reveals that the sub-bands have their origin in the short-range antiferromagnetic correlations that become enhanced at low temperatures. These conclusions about the half-filled state are strengthen by the result obtained using an increased cluster size $N_c = 4$ (plaquette). The local spectral function, i.e. the cluster density of states (DOS), is shown in Fig. 2 for $U = 4t$ and $T = 0.15t$. Notice that the change in cluster size does not modify the qualitative behavior of the solution.

Next, we examine the evolution of the Mott insulator upon doping. A comparison of the frequency dependence of the local cluster spectral function for three different filing values is shown in Fig. 3. The most striking feature of the finite doping spectral functions is the presence of a pseudogap in vicinity of the Fermi energy, as evidenced by the corresponding suppression of the spectral weight for $n = 0.95$ (red curve in Fig. 3) and $n = 0.9$ (green line). This feature is distinct from the Mott gap which becomes a shallow minimum and moves at higher energies. Notice that the pseudogap does not fill in upon doping, but rather moves toward higher frequencies until, eventually, this feature will be replaced at the Fermi level by the narrow peak of the lower Hubbard band. At the same time, the corresponding narrow feature of the upper Hubbard band loses weight as the doping increases. In order to better characterize the pseudogap, let us analyze its temperature dependence. A plot of the local cluster spectral function $A_{11}(\omega)$ for three different temperatures is shown in Fig. 4. The pseudogap disappears when the temperature is raised above a critical value which in this case is roughly $0.27t$. This temperature is related to the
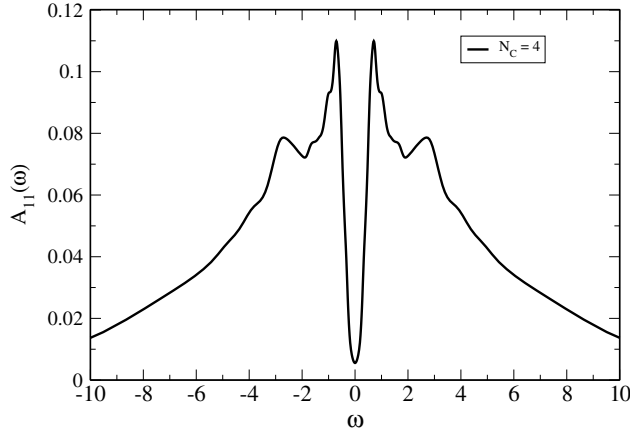
Fig. 2. Cluster density of states for a half-filled two-dimensional Hubbard model with $U = 4t$ using a four site cluster (plaquette) CDMFT with NCA solver. The temperature is $T = 0.15t$.
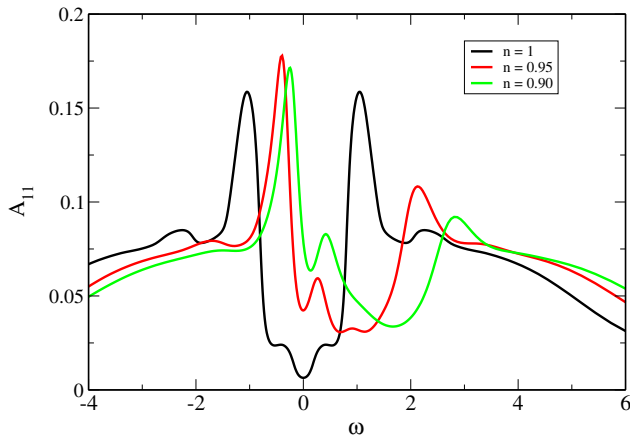

Fig. 3. Doping evolution of the frequency dependent local spectral function for the two-dimensional Hubbard model with $U = 5t$ at a temperature $T = 0.2t$. The black curve represents the half-filled case ($n = 1$), red corresponds to $n = 0.95$ and green is for $n = 0.9$. The results are obtained using a two-site CDMFT with NCA solver. (For interpretation of the references to color in this figure legend, the reader is referred to the web version of this paper.)

width of the pseudogap that is defined by an energy scale proportional with the distance between the two peaks neighboring the gap. As the origin of these peaks can be traced back [38] to the formation of local singlet (left peak) and triplet (right peak) states in the cluster, the distance between them is roughly equal to the bare single–triplet splitting [38], J. For $U = 5t$ and $N_c = 2$ this splitting is about $0.7t$, while in the limit of large interaction strength we have $J \approx 4t^2/U$. To verify our conclusions, first we increase the strength of the interaction from $U = 5t$ to $U = 8t$. As shown in Fig. 5, we observe a significant reduction of the pseudogap, consistent with the change in J_{eff} from $0.7t$ to about $0.45t$.

Fig. 4. Frequency dependence of the cluster density of states for $n = 0.95$ and three different temperatures: $T = 0.3t$ (black), $T = 0.2t$ (red), and $T = 0.15t$ (green). The other parameters are the same as in Fig. 3. (For interpretation of the references to color in this figure legend, the reader is referred to the web version of this paper.)
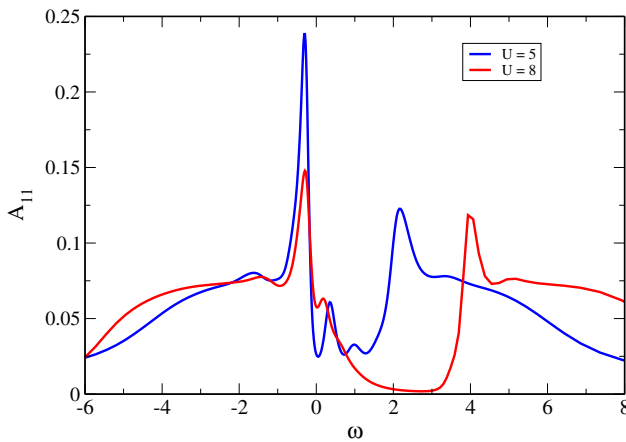

Fig. 5. Comparison between the cluster DOS of the two-dimensional Hubbard model with $U = 5t$ (blue line) and $U = 8t$ (red line). The filling is $n = 0.95$ and the temperature is $T = 0.15t$. The solutions were obtained using two site CDMFT with NCA solver. (For interpretation of the references to color in this figure legend, the reader is referred to the web version of this paper.)

Next, we modify the size of the cluster from $N_c = 2$ to $N_c = 4$. A comparison between the local spectral functions obtained within these approximations is shown in (Fig. 6). We notice the same qualitative features in both cluster solutions and the fact that the quantitative differences are significant. These differences provide an estimate for the order of magnitude of the errors that we expect for the link approximation. Using the plaquette approximation we compare again the local spectral functions for two different values of the on site interaction, $U = 8t$ and $U = 16t$. The comparison is shown in (Fig. 7) while in (Fig. 8) we plot the spectral function in the pseudogap regime for different temperatures.

Fig. 6. Cluster DOS for the two-dimensional Hubbard model with $U = 8t$ and $n = 0.95$. The blue line represents a two-site cluster approximation, while the red line was obtained using a four sites cluster. We used a CDMFT + NCA method and the temperature is set at $T = 0.15t$. (For interpretation of the references to color in this figure legend, the reader is referred to the web version of this paper.)
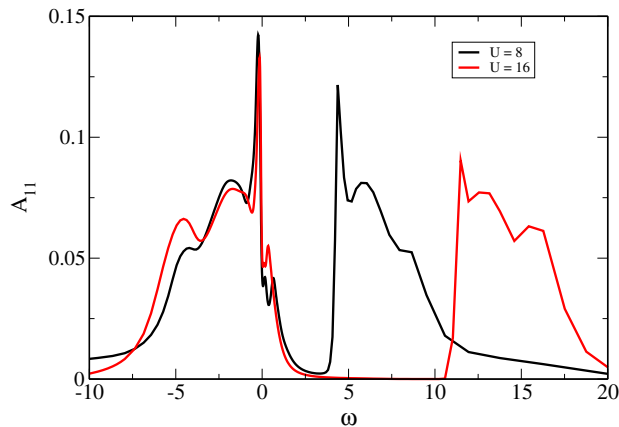

Fig. 7. Frequency dependence of the local spectral function for the 2D Hubbard model with $U = 8t$ (black) and $U = 16t$ (red). The filling is $n = 0.95$ and the temperature $T = 0.08t$. We used four-sites CDMFT + NCA. (For interpretation of the references to color in this figure legend, the reader is referred to the web version of this paper.)

As we lower the temperature, the details of the local spectral function in the vicinity of the Fermi energy start to emerge. As U is large, we approach the asymptotic behavior with $J \approx 4t^2/U$, i.e. approximately 0.25 in this case. As (Fig. 8) shows clearly, the pseudogap, defined as the minimum between the two peaks on both sides of zero frequency, is indeed of order J. While the details of the spectral function in the region relevant for the pseudogap may not be easy to resolve, especially when J is small, the temperature at which we see for the first time a minimum gives a good indication about the energy scale relevant for this phenomenon. The data from both (Figs. 8 and 4) is consistent with a critical temperature which is about $T_J = J/3$.
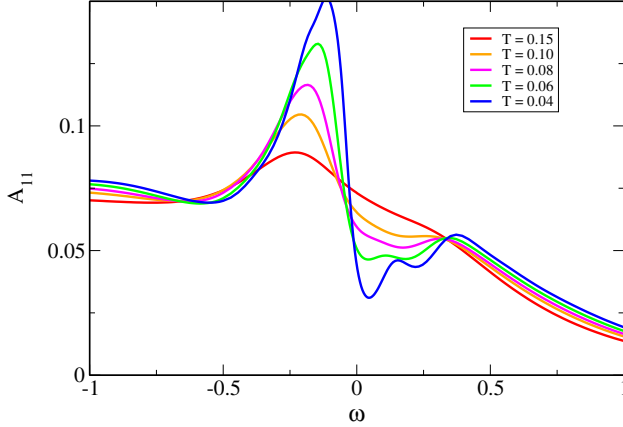
Fig. 8. Temperature evolution of the pseudogap in the 2D Hubbard model with $U = 16t$ and $n = 0.95$. (Four-sites CDMFT + NCA calculation).

4. Lattice quantities and the zeros of the Green function

A cluster DMFT approach consists of two main steps, the self-consistent determination of the cluster impurity solution and the re-construction of the lattice quantities. Some physical results that can be extracted directly from the cluster solution were presented in the previous Section. Now we will focus on the problem of re-constructing the lattice quantities from their cluster counterparts and will present a series of results that reveal a more refined physical picture of the pseudogap state.

4.1. Short range self-energies versus short-range cumulants

We start by investigating the periodization procedures described in Section 2. In particular we want to find the optimal scheme for reconstructing the lattice quantities for systems in or near the Mott phase. To benchmark our method, we analyze the half-filled one-dimensional Hubbard model with nearest neighbor hopping within a CDMFT scheme for two sites or four sites clusters using an exact diagonalization (ED) impurity solver. Before presenting the results, let us notice that the zero temperature Green's function in a Mott insulator is characterized by a gap at the Fermi level, i.e. $\text{Im}\, G(\mathbf{k}, \omega) = 0$ for frequencies in the vicinity of $\omega = 0$. In addition, from the spectral representation of the Green's function we get for the zero frequency real part of G the expression

$$\text{Re}\, G(\mathbf{k}, 0) = \frac{1}{\pi} \int_{-\infty}^{-\varDelta} \frac{\text{Im}\, G(\mathbf{k}, x)}{x}\, dx + \frac{1}{\pi} \int_{\varDelta}^{\infty} \frac{\text{Im}\, G(\mathbf{k}, x)}{x}\, dx. \tag{24}$$

Since the spectral function $\sigma(k, 0) = 1/\pi\, \text{Im}\, G(k, 0)$ of the half-filled one dimensional Hubbard model is symmetric for $k = \pm\pi/2$, $\sigma(\pm\frac{\pi}{2}, x) = \sigma(\pm\frac{\pi}{2}, -x)$, the two integrals in Eq. (24) completely cancel each other and we have

$$G\left(k = \pm\frac{\pi}{2}, \omega = 0\right) = 0, \tag{25}$$

i.e. the interacting Green function has **zeros** [42] at momenta corresponding to the non-interacting Fermi points. Consequently, the corresponding self-energies will diverge. Our goal is to identify the periodization procedure that better reproduces these features. To this end, we calculate the lattice Green's function $G_{ij}(i\omega_n)$ on the Matsubara axis using 2-site and 4-site cluster approximations and compare the results obtained by applying the self-energy and the cumulant periodization schemes. Due to the symmetry of the spectral functions, $G_{ij}(i\omega_n)$ is real for $|R_i - R_j|$ odd and imaginary for $|R_i - R_j|$ even. Shown in (Fig. 9) is the local lattice Green's function $G_{11}(i\omega_n)$. We notice that the cumulant solution correctly reproduces the low-energy behavior expected for the Green function in the presence of a gap, i.e. $G_{11}(\omega_n) \approx \text{const} \times \omega_n$. In contrast, the self-energy solution has a finite zero frequency value proportional to the density of states of a fictitious $\pm\pi/2$ quasiparticle. In addition, the cumulant curves for $N_c = 2$ (orange) and $N_c = 4$ (red) are almost on top of each other, signaling a high degree of convergence of the solution even for small clusters. This supports the assumption of the cumulant scheme, i.e. that cumulants are short-range quantities in the Mott phase. In contrast, although the self-energy solution converges toward the cluster solution as we increase the cluster size, one would need an infinite cluster to rigorously recover the correct qualitative behavior. These conclusions are supported by higher order even parity Green's functions. On the other hand, the behavior of the odd parity components is exemplified by the nearest neighbor Green's function shown in (Fig. 10). Although quantitatively the two solutions are comparable, qualitatively they differ: the cumulant solution (red and orange lines) correctly reproduces the low energy limit, $G_{12}(\omega_n) \approx G_{12}(0) + \text{const} \times \omega_n^2$, while the self-energy solution has a non-zero slope at $\omega_n = 0$ as a consequence of the spurious $k = \pm\pi/2$ quasiparticles. We can conclude that: (1) There is no significant **quan-**
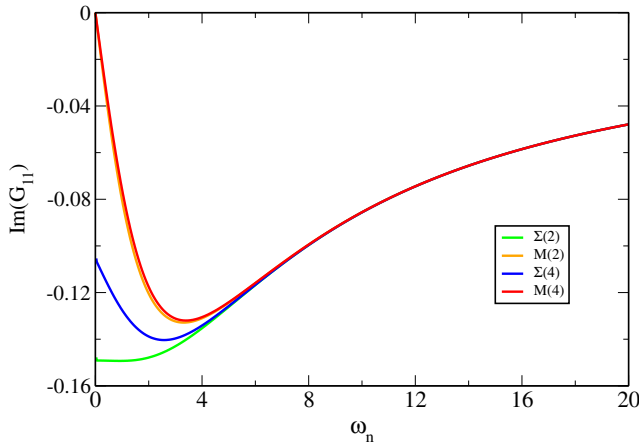

Fig. 9. Imaginary frequency dependence of the imaginary part of the local lattice Green function (real part identically zero) for the half-filled 1D Hubbard model with $U = 8t$. The green and blues lines are obtained by periodizing the self-energy within a 2-site and a 4-site cluster CDMFT, respectively. The orange ($N_c = 2$) and red ($N_c = 4$) lines are obtained by periodizing the cumulant. The vanishing zero frequency Green function (cumulant solution) is a signature of the Mott gap, while the finite values of the self-energy solutions are determined by the spurious quasiparticles at $\pm\pi/2$. The results were obtained using a zero temperature exact diagonalization impurity solver. (For interpretation of the references to color in this figure legend, the reader is referred to the web version of this paper.)
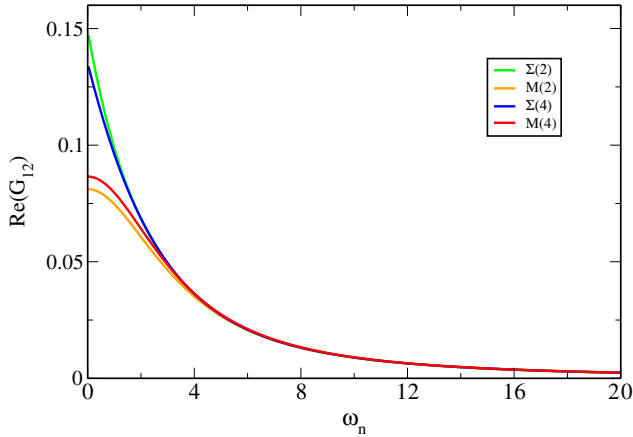
Fig. 10. Imaginary frequency dependence of the real part of the nearest neighbor lattice Green function (the imaginary part of G_{12} is identically zero). Same color code an parameters as in Fig. 9.

titative difference between the cumulant and the self-energy solutions for the nearest neighbor Green's function. They converge, from below and above, respectively, to the real solution the lays in between the two families of curves. (2) There is a major **qualitative** difference between the two solutions as the assumption that the self-energy is a local quantity fails to reproduce the correct low energy behavior. To support our statement that the real solution lays in between the families of cumulant and self-energy solutions, we notice that $\mathrm{Re}\,G_{12}$ is related to the kinetic energy of the Hubbard model which can be determined using the Bethe ansatz. In (Fig. 11), we compare the Bethe ansatz result (red line), with the kinetic energy extracted from the lattice G_{12} obtained using the cumulant scheme (magenta) and the self-energy periodization (blue line with triangles). We also include the Green's function periodization scheme (green line with squares) and the kinetic energy obtained directly from the cluster nearest neighbor Green's function. First, notice that the cumulant and self-energy results represent indeed lower and upper bounds for the exact solution. In fact the average of the two estimates for the kinetic energy, K, represents an excellent approximation for the exact result for any value of the on-site interaction, as shown in the inset of (Fig. 11) where the deviation $\Delta E_{Kin} = K_{BA} - 1/2(K_M + K_\Sigma)$ is represented as a function of U. Second, notice that the values of the kinetic energy given by the cluster Green's function (black) are significantly different from the exact result, while the curves obtained using the lattice Green's function, extracted using various procedures, cluster around the Bethe ansatz line. Also, the results obtained by periodizing the Green's function (green) and those obtained by periodizing the cumulant (magenta) are remarkably similar, especially in the strong coupling regime. This analysis shows clearly that in any small cluster DMFT scheme observables should be always extracted from the physical lattice quantities and not from their cluster counterparts.

To get further insight, we study the momentum dependence of the zero frequency lattice Green's function,

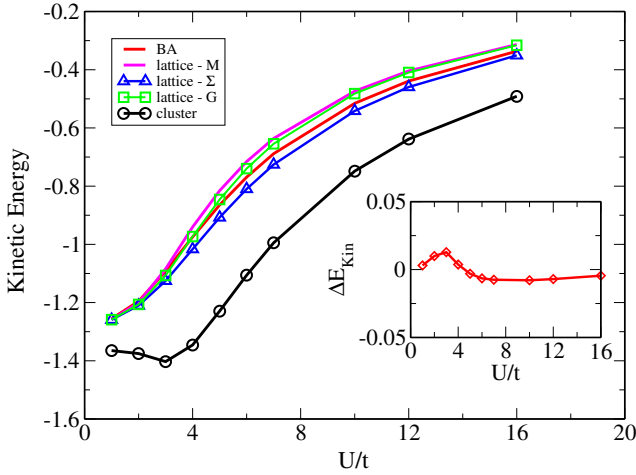$$G(\mathbf{k}, 0) = -\frac{1}{r(k) + i\eta(k)}, \tag{26}$$

Fig. 11. Kinetic energy of the half-filled one-dimensional Hubbard model as a function of the on-site interaction U at zero temperature using: the Bethe ansatz (red line), the cluster Green's function (black circles) and the lattice Green's function obtained by periodizing G (green squares), the self-energy (blue triangles) and the irreducible cumulant (magenta line). The results are obtained using two site CDMFT and an exact diagonalization impurity solver. Inset: the difference between the exact result and the average of the cumulant and self-energy solutions. (For interpretation of the references to color in this figure legend, the reader is referred to the web version of this paper.)

where $r(k) = \epsilon(k) + \text{Re}\,\Sigma(k,0)$ represents the renormalized band energy and $-\eta(k)$ is the imaginary part of the zero frequency self-energy. As we mentioned at the beginning of this section, the self-energy, and consequently $r(k)$, is singular at $k = \pm\pi/2$, while $\eta(k)$ vanishes everywhere, except the singularity points, due to the presence of the Mott gap. To explore how these features are reproduced by the periodization schemes, we calculate the renormalized energy and compare in (Fig. 12) the self-energy periodization procedure (green line for a 2-site cluster and blue line for a 4-site cluster) with the cumulant periodization procedure (orange line for $N_c = 2$ and red line for $N_c = 4$). We observe that the cumulant periodization correctly reproduces the divergence of the self-energy, i.e. the **zero** of the Green function, at $k = \pi/2$. In contrast, the self-energy periodization produces a zero of the renormalized energy, i.e. a **pole** in the Green function. In addition, increasing the cluster size does not change qualitatively the cumulant solution but produces small quantitative corrections. The corrections to the self-energy solution determine a slow convergence to the cumulant solution starting with momenta far from the singularity (see the inset of Fig. 12). Notice that in the vicinity of $k = \pi/2$ $r(k)$ should diverge as const$/(k - \pi/2)$. This behavior is correctly reproduced by the cumulant solution, while the self-energy solution is totally unphysical. The real solution has to have a negative slope in the vicinity of $\pi/2$, but the self-energy solution for $N_c = 2$ has a positive slope everywhere. The situation does not improve much for $N_c = 4$ (except for small values of k, as shown in the inset). The fact that the self-energy solution is not changing much as you go from $N_c = 2$ to $N_c = 4$ does not mean that it is almost converged, but rather that the convergence is very slow. This is not so surprising because the underlying assumption (i.e. finite range self-energy) totally contradicts the physical reality (infinite range self-energy).
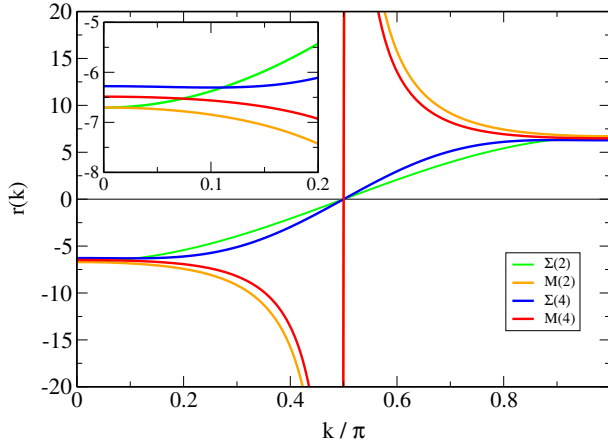
Fig. 12. Renormalized energy as a function of momentum for the 1D half-filled Hubbard model with $U = 8t$. The green and blues lines are obtained by periodizing the self-energy within a 2-site and a 4-site cluster CDMFT, respectively. The orange ($N_c = 2$) and red ($N_c = 4$) lines are obtained by periodizing the cumulant. The inset shows the behavior at small momenta. Exact diagonalization was used to solve the effective impurity problem. (For interpretation of the references to color in this figure legend, the reader is referred to the web version of this paper.)

The conclusion of the present analysis of the half-filled one-dimensional Hubbard model is that a CDMFT scheme using cumulants as the basic irreducible quantities for re-constructing the lattice Green's function correctly reproduces the qualitative features of the solution for any cluster size, beyond any uncertainty associated with the resolution of the approximation. In contrast, a solution based on the assumption that the self-energy is a local quantity, fails to reproduce the zero of the Green function at ($k_0 = \pm\pi/2$, $\omega = 0$) and zero temperature. Instead, this assumption generates poles in the Green function with a residue Z_{k_0} that vanishes only in the limit of infinite cluster size. The physical reason for this behavior is that the zero frequency self-energy in a Mott insulator is not a local quantity. The short-range quantity that has to be used for describing such a system in any DMFT cluster scheme is the cumulant. The signature of this property in the numerical solution can be seen already in the cluster quantities, i.e. before introducing any periodization procedure. For our 1D system at half filling treated in a four site cluster approximation, the shortest range non-vanishing zero frequency self-energies (or cumulants) are the nearest neighbor and the third-order neighbor components. Calculating the ratio between the **cluster** average of these components we obtain

$$\frac{\Sigma_{14}}{2/3\,\Sigma_{12} + 1/3\,\Sigma_{23}} = -0.531029, \tag{27}$$

$$\frac{M_{14}}{2/3\,M_{12} + 1/3\,M_{23}} = -0.0926043. \tag{28}$$

This clearly shows that the cumulant is a short-range quantity that rapidly decreases as the distance $|R_i - R_j|$ increases, while the self-energy is not. Therefore, in the presence of Mottness, it is the cumulant that represents the natural quantity to be used in the CDMFT super-lattice construction and the subsequent re-construction of the lattice quantities.

To further emphasize our point we show in Fig. 13 the distance dependence of the zero frequency **lattice** self-energy obtained using the cumulant scheme for the $N_c = 4$ cluster. These self-energies are obtained by Fourier transforming the lattice $\Sigma(k, 0)$ constructed using the cumulant periodization scheme. We have to recall that, at zero frequency, all the even parity functions are zero by symmetry, therefore we show only the odd parity self-energy components (normalized by Σ_{12}). The figure shows clearly that the self-energy cannot be considered a short-range quantity. In contrast, the cumulant practically vanishes within a few lattice sites. This is illustrated by the small ratio of the only two non-zero components, i.e. with odd parity and a range smaller than the cluster size, that we have in this approximation, M_{14}, and M_{12}.

Turning now to the two-dimensional (2D) case, we note that all the qualitative features discussed above can be observed in the CDMFT solution for a 2D half-filed Hubbard model. In particular, we can estimate the kinetic energy using either the nearest neighbor cluster Green's function, or its lattice correspondent obtained with various periodization schemes. The results are shown in (Fig. 14) which represents the 2D analog of the one dimensional analysis presented in (Fig. 11). Notice that, again, the values obtained from the lattice Green's function are very similar, especially those given by the cumulant and Green's function periodization schemes, while the cluster estimate is significantly different re-enforcing our conclusion about the necessity of the lattice re-construction step. On the other hand, the failure of the self-energy construction to capture correctly the Mott physics can be illustrated by calculating the local spectral function $A_{11}(\omega) = -1/\pi \text{Im} \, G_{11}(\omega)$, i.e. the density of states (DOS), for the half-filled Hubbard model. The results obtained using a four cluster CDMFT with exact diagonalization impurity solver are shown in (Fig. 15) for a model with $U = 16t$. The large value of the on-site interaction should produce a sizable Mott–Hubbard gap, which is clearly visible in the cluster solution (black line). While the cumulant scheme (red line) generates indeed a cluster local spectral func-
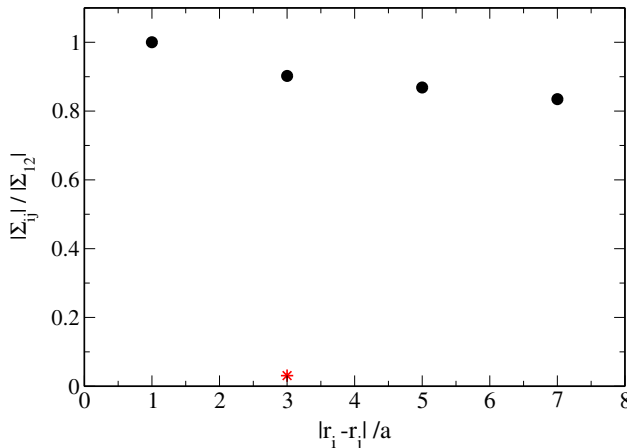

Fig. 13. Absolute value of the zero frequency ratio Σ_{ij}/Σ_{12} as a function of $|R_i - R_j|$ in lattice units. For comparison we show the only ratio that is non-zero in this approximation for the lattice cumulants, $|M_{14}|/|M_{12}| = 0.0308681$ (red star). The **lattice self-energy** of the 1D half-filled Hubbard model ($U = 8t$, $T = 0$) **is not a short range** quantity, while the **cumulant is**. (For interpretation of the references to color in this figure legend, the reader is referred to the web version of this paper.)
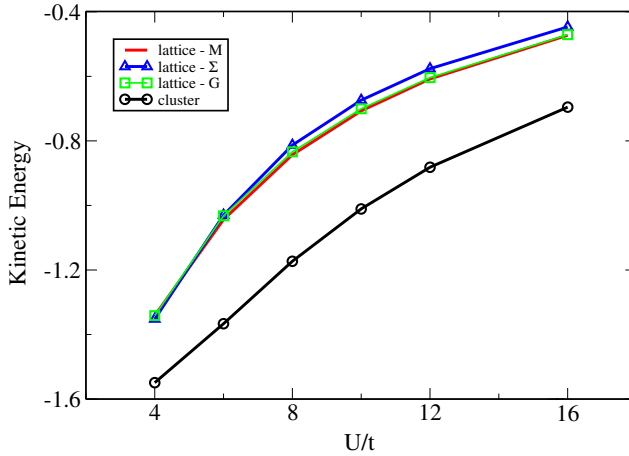
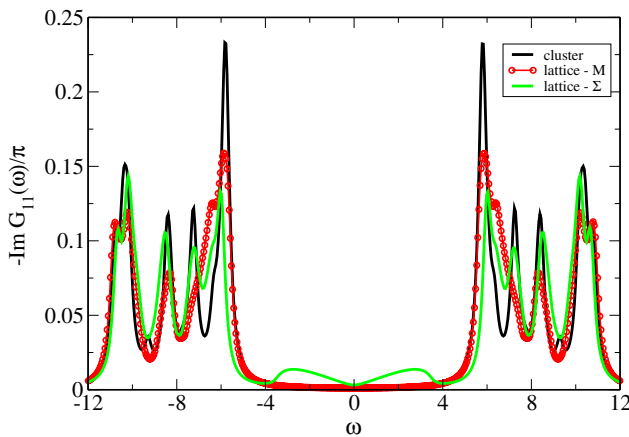Fig. 14. Kinetic energy of the half-filled 2D Hubbard model as a function of the on-site interaction U at zero temperature using: the cluster Green's function (black circles) and the lattice Green's function obtained by periodizing G (green squares), the self-energy (blue triangles) and the irreducible cumulant (red line). The results are obtained using four site CDMFT (plaquette) and an exact diagonalization impurity solver. (For interpretation of the references to color in this figure legend, the reader is referred to the web version of this paper.)

Fig. 15. Density of states as a function of frequency for the half-filled 2D Hubbard model with $U = 16t$ at zero temperature. The black line represents the local density of states for the cluster, the red circles were obtained by periodizing the cumulant, while the green line is given by the periodization of the self-energy. The results are obtained within a plaquette CDMFT + ED approach. (For interpretation of the references to color in this figure legend, the reader is referred to the web version of this paper.)

tion that exhibits a well defined gap, the self-energy reconstruction scheme (green line) generates spurious states within the gap. These states are obviously not physical and they signal the failure of the procedure at half filling. We note that the local cluster quantities are expected to be reasonable estimates for the corresponding lattice quantities, even in the case of small clusters. In fact, in the Green's function periodization scheme the values of

$G_{11}(\omega)$ for the lattice and the cluster coincide and are both represented by the black curve in (Fig. 15). The same identity holds for the cluster and lattice local cumulants in the cumulant periodization scheme. However, the agreement between the local lattice Green's function obtained in the cumulant scheme and the local cluster Green's function is not a trivial result and it reveals that the underlying assumption of a short-range cumulant is correct.

To test the validity of the re-construction schemes away from half filling we calculate the doping dependence of the chemical potential for the 2D Hubbard model at finite temperature. As shown in (Fig. 16) the filling derived from the lattice Green's function obtained with the cumulant scheme agrees nicely with the cluster filling. In contrast, the self-energy periodization scheme produces significant deviations for doping values smaller than 20%, signaling the failure of the underlying assumption in this regime. At large doping all the periodization schemes converge, revealing the fact that the local components of both the self-energy and the cumulant are much larger than the non-local components. On the contrary, in the Mottness regime close to half-filling, the non-local components of the self-energy cannot be neglected. To further substantiate our claim that, even away from half-filling in the small doping regime, the short-range irreducible quantity that is appropriate for a cluster DMFT description of the Hubbard model is the cumulant, rather than the self-energy, we compare in Fig. 17 the local spectral functions obtained using the cumulant and the self-energy periodization schemes within a CDMFT approach for $N_c = 2$ and $N_c = 4$. Our previous conclusions are supported by the good agreement between the lattice Green functions obtained with the cumulant periodization scheme (red lines) and their cluster counterparts (black). In contrast, the self-energy method produces a qualitatively different result characterized by the filling of the Hubbard gap and the absence of the pseudo-gap feature near the Fermi level. Not surprisingly, the discrepancy is stronger for $N_c = 2$ and becomes weaker as we increase the cluster size. Also notice
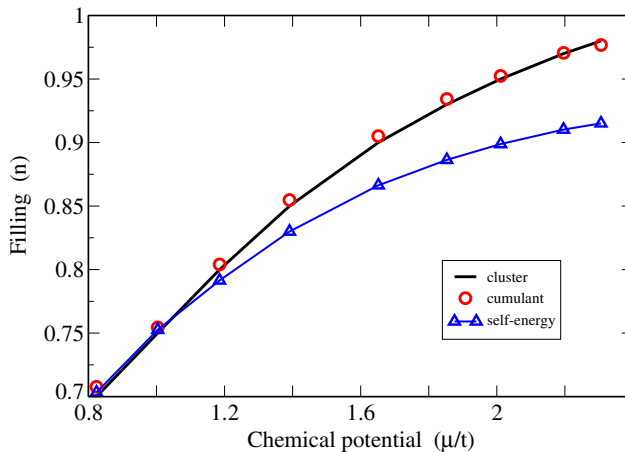

Fig. 16. Density as a function of chemical potential, μ, for the 2D Hubbard model with $U = 8t$ at a temperature $T = 0.1t$. The black line represents the filling of the cluster, while the filling of the lattice is given by the red circles (if we periodize the cumulant) or the blue triangles (if we periodize the self-energy). The results were obtained using a plaquette CDMFT + NCA approach. (For interpretation of the references to color in this figure legend, the reader is referred to the web version of this paper.)
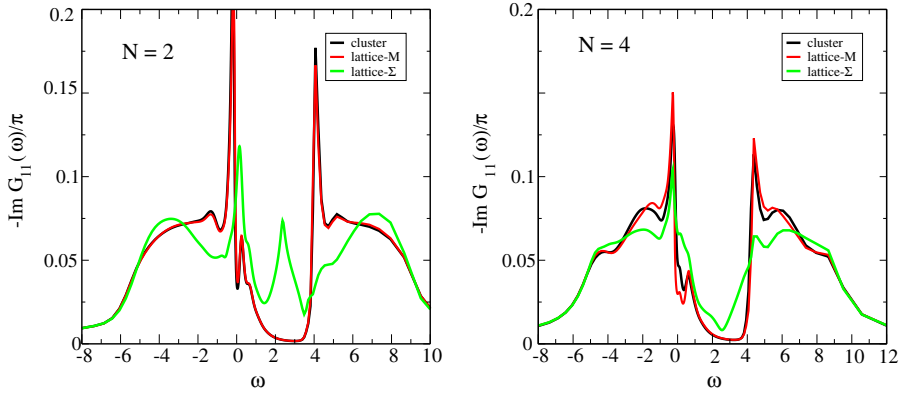
Fig. 17. Comparison between the local spectral functions for the 2D Hubbard model extracted from the cluster Green's function (black) and the lattice Green's functions obtained by periodizing the cumulant (red) and the self-energy (green), We used a CDMFT scheme with NCA solver for clusters with $N_c = 2$ (left panel) and $N_c = 4$ (right panel). The parameters of the calculation are $U = 8t$, $n = 0.95$ and $T = 0.15t$, where t is the near-neighbor hopping. The (real) frequency ω is also expressed in units of hopping. (For interpretation of the references to color in this figure legend, the reader is referred to the web version of this paper.)

that the main qualitative features of the cumulant result are independent of the cluster size, while the self-energy solution varies strongly with N_c.

4.2. Mottness and the hidden zeros of the Green's function

The next goal is to identify the consequences of our analysis of the re-construction schemes and of their underlying assumptions for the low energy properties of a correlated metal in the proximity of a Mott phase. To this end, we investigate the structure and properties of the zero frequency Green's function $G(\mathbf{k}, 0)$ for the 2D Hubbard model with nearest neighbor hopping using the CDMFT approach. To have a better grasp of the physical meaning of our results, let us derive the explicit expression for the renormalized energy $r(k)$ (see Eq. (26)) in terms of cluster self-energies.

In order to take full advantage of the symmetry properties of the cluster, it is convenient to consider instead of the usual matrix elements W_{ij} labeled by the site indices, combinations that can be labeled by the irreducible representations of the point group determined by the symmetry of the cluster. In the case of a plaquette ($N_c = 4$), the corresponding point group is D_4 which has four one-dimensional irreducible representations (A_1, A_2, B_1, B_2) and one two-dimensional representation (E). Using the notations W_0, W_1, and W_2 for the local, link, and diagonal components, respectively, we can define

$$
\begin{aligned}
W_A &= W_0 - W_2, \\
W_B &= W_0 - 2W_1 + W_2, \\
W_C &= W_0 + 2W_1 + W_2,
\end{aligned}
\tag{29}
$$

where $W_A \equiv W(E, E) = W(E', E')$ is double degenerate and can be indexed using the two-dimensional representation of the symmetry group, while $W_B \equiv W(B_1, B_1)$ and $W_C \equiv W(A_1, A_1)$. In terms of the combinations defined by Eq. (29) all cluster matrices are diagonal and we can write easily the cluster cumulants in terms of cluster self-energies,

$$M_A(\omega) = \frac{1}{\omega + \mu - \Sigma_A(\omega)},$$

$$M_B(\omega) = \frac{1}{\omega + \mu - \Sigma_A(\omega)}, \tag{30}$$

$$M_C(\omega) = \frac{1}{\omega + \mu - \Sigma_A(\omega)}.$$

Using the diagonal cluster cumulants, the expression (23) for the periodized lattice cumulant becomes

$$M(\mathbf{k}, \omega) = M_A(\omega) S_A(\mathbf{k}) + M_B(\omega) S_B(\mathbf{k}) + M_C(\omega) S_C(\mathbf{k}), \tag{31}$$

where the momentum dependent $S_X(\mathbf{k})$ functions are

$$S_A(\mathbf{k}) = \frac{1}{2}[1 - \cos(k_x)\cos(k_y)],$$

$$S_B(\mathbf{k}) = \frac{1}{4}[1 - \cos(k_x) - \cos(k_y) + \cos(k_x)\cos(k_y)], \tag{32}$$

$$S_C(\mathbf{k}) = \frac{1}{4}[1 + \cos(k_x) + \cos(k_y) + \cos(k_x)\cos(k_y)].$$

Notice that $0 \leqslant S_X \leqslant 1$ and $S_A + S_B + S_C = 1$ for any k-vector in the Brillouin zone. In addition, for $\mathbf{k} = (0,0)$ we have $S_C = 1$ while the other two functions vanish so that $M(\mathbf{k} = (0,0), \omega) = M_C(\omega)$, i.e. the origin is controlled by the 'C' component. The other two components control the (π, π) point (B) and $(0, \pi)$ point (A), as well as the points related with them by symmetry. Introducing now Eq. (30) into Eq. (31) and using the general relation between the lattice cumulant and the lattice self-energy, $M = 1/(\omega + \mu - \Sigma)$, we obtain the expression of the lattice self-energy in terms of cluster self-energies within the cumulant periodization scheme

$$\Sigma(\mathbf{k}, \omega) = \omega + \mu - \left[\frac{S_A(\mathbf{k})}{\omega + \mu - \Sigma_A(\omega)} + \frac{S_B(\mathbf{k})}{\omega + \mu - \Sigma_B(\omega)} + \frac{S_C(\mathbf{k})}{\omega + \mu - \Sigma_C(\omega)} \right]^{-1}. \tag{33}$$

This relation is highly non-linear, in contrast with Eq. (22) obtained within the short range self-energy assumption. The implications of the assumptions about the range of the irreducible quantities for the low-energy physics of a correlated metal become now transparent. In the limit of zero temperature, the imaginary parts of the cluster self-energies vanish, as we will show bellow, so that the zero frequency Green's function (26) depends only on the renormalized energy $r(\mathbf{k})$ that can be expressed within the self-energy and cumulant periodization schemes as

$$r^{(\Sigma)}(\mathbf{k}) = \epsilon(\mathbf{k}) - \mu + \operatorname{Re}\Sigma_A(0) S_A(\mathbf{k}) + \operatorname{Re}\Sigma_B(0) S_B(\mathbf{k}) + \operatorname{Re}\Sigma_C(0) S_C(\mathbf{k}), \tag{34}$$

$$r^{(M)}(\mathbf{k}) = \epsilon(\mathbf{k}) + \left[\frac{S_A(\mathbf{k})}{\operatorname{Re}\Sigma_A(0) - \mu} + \frac{S_B(\mathbf{k})}{\operatorname{Re}\Sigma_B(0) - \mu} + \frac{S_C(\mathbf{k})}{\operatorname{Re}\Sigma_C(0) - \mu} \right]^{-1}. \tag{35}$$

In principle, there are two possible regimes for the interacting system. In the first regime, the diagonal cluster self-energies are dominated by the local component, or more precisely by $\operatorname{Re}\Sigma_0 - \mu$, while the non-local components $\operatorname{Re}\Sigma_{1(2)}$ represent small correction. In this case, Eq. (35) reduces in the first approximation to Eq. (34) and the only effect of the interactions is to renormalize the bare energy band by dynamically generated hopping terms,

$t_{\text{eff}} = t + \text{Re}\,\Sigma_1(0)$ and $t'_{\text{eff}} = \text{Re}\,\Sigma_2(0)$. In this regime all the periodization schemes converge and, in fact, the single-site DMFT represents a good first-order approximation. In the Hubbard model this regime is realized for large doping values, for example $x > 20\%$ for $U = 8t$. In contrast, in the second regime, close to the Mott insulating phase, the non-local components of the self-energy become comparable or larger than $\text{Re}\,\Sigma_0 - \mu$ and the self-energy re-construction scheme fails. Moreover, the denominators in the right hand side of Eq. (35) may acquire opposite signs generating divergences of the renormalized energy $r(k)$, or, equivalently, zeros of the Green's function. In the remaining of this Section we discuss in detail the appearance of these zeros and their connection with the opening of the pseudogap at the Fermi level, and, based on this analysis, we provide a simple picture for the formation of Fermi arcs.

We mentioned above that the imaginary parts of the cluster self-energies at zero frequency can be neglected in the limit of zero temperatures. To support our claim, we present in (Fig. 18) the imaginary parts of the diagonal cluster self-energies as functions of the Matsubara frequency for a two-dimensional Hubbard model with $U = 8t$ for a filling $n = 0.93$. The tendency of the self-energy to vanish in the limit of zero frequency can be observed, within the resolution of our numerical methods, for all doping values, the major difference being that the slope of the curves at small frequencies increases as we approach the Mott insulator [20]. While the imaginary parts of the self-energy are negligible, the real parts, more precisely $\text{Re}\,\Sigma_X(0) - \mu$, are strongly dependent on doping. In (Fig. 19), we show the 'A' and 'C' diagonal components versus the chemical potential for the two dimensional Hubbard model. The third component, 'B' (not shown) is always positive. We can easily recognize the two regimes: one, characterized by a short-range self-energy, for $\mu < 1.4$, which corresponds to roughly 20% doping for our system, where the local self-energy dominates and the diagonal components tend to become equal, and the other governed by Mottness and dominated by the non-local self-energies. The relevant zero frequency quantities for the large doping regime are shown in (Fig. 20) for a system with
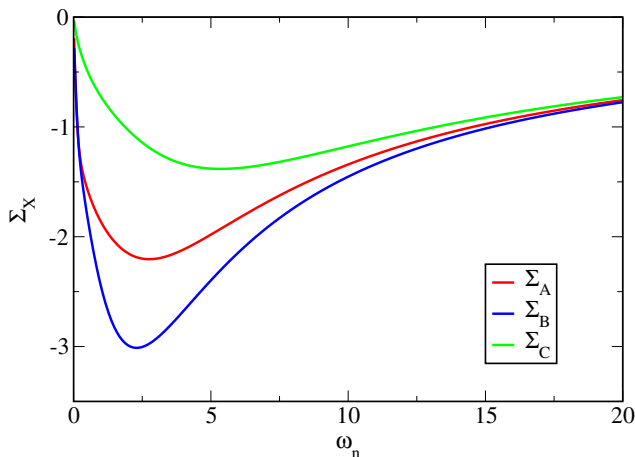

Fig. 18. Imaginary parts of the diagonal cluster self-energies as functions of the Matsubara frequency. The calculation was done for a 2D Hubbard model with $U = 8t$ for a filling $n = 0.93$ at $T = 0$ using a four site CDMFT + ED.
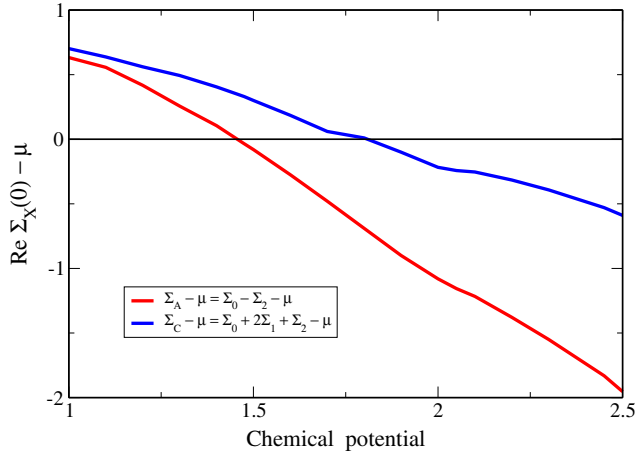
Fig. 19. Real parts of the diagonal cluster self-energies versus chemical potential for the 2D Hubbard model with $U = 8t$. The calculation was done using a four sites CDMFT + ED. Notice the change in sign for $\mathrm{Re}\,\Sigma_A - \mu$ at $\mu = 1.47$, and for $\mathrm{Re}\,\Sigma_B - \mu$ around $\mu = 1.8$. The 'B' component (not shown) is always positive.

22% doping. We notice that, indeed, the two periodization schemes give almost identical results for $r(\mathbf{k})$ so that the corresponding curves, red (cumulant) and green (self-energy), are almost indistinguishable. The points where $r(\mathbf{k})$ vanishes correspond to the quasiparticle poles of the Green's function. The locus of these points in the Brillouin zone represents the Fermi surface which, in this case, is a large electron-type surface (blue line in the lower left panel). The Fermi surface can also be observed in the spectral function $A(\mathbf{k}, 0)$ and corresponds to the location of the maxima (red color in the lower right panel). We can conclude that in this regime the system is a Fermi liquid and that the corrections due to short-range correlations are small.

As we approach the Mott insulator, the short-range correlations become more and more important and start to modify the physics. Within our approximation, the first signature of this new physics occurs around 20% doping, when the diagonal component $\mathrm{Re}\,\Sigma_A - \mu$ changes sign (see Fig. 19). Shown in (Fig. 21) is the renormalized energy for a system with 18% doping. The renormalized energy $r(\mathbf{k})$ (red curve) starts to develop singularities in certain points of the Brillouin zone corresponding to zeros of the Green's function. Notice that the singularities occur in regions far from the Fermi surface, i.e. from the points where r vanishes. For comparison, we also plotted the $r(\mathbf{k})$ obtained within the self-energy re-construction scheme (green curve), which fails in this regime. The assumption that the self-energy is short range will always generate a normal Fermi liquid with poles but no zeros in the Green's function. The emergence of lines of zeros in the Green's function at zero energy described here is similar to that found by several groups in quasi one-dimensional systems [39–41,43].

If we continue to reduce the doping, the system becomes more and more incoherent and, eventually, the quasiparticles disappear. This evolution is illustrated in (Figs. 22 and 23). In Fig. 22, we observe that for $n = 0.92$ $r(\mathbf{k})$ still vanishes in the vicinity of $(\pi/2, \pi/2)$, while in the vicinity of $(\pi, 0)$ the curve "sinks" below the Fermi level indicating the absence of a Fermi surface in that region of the Brillouin zone. In addition to the
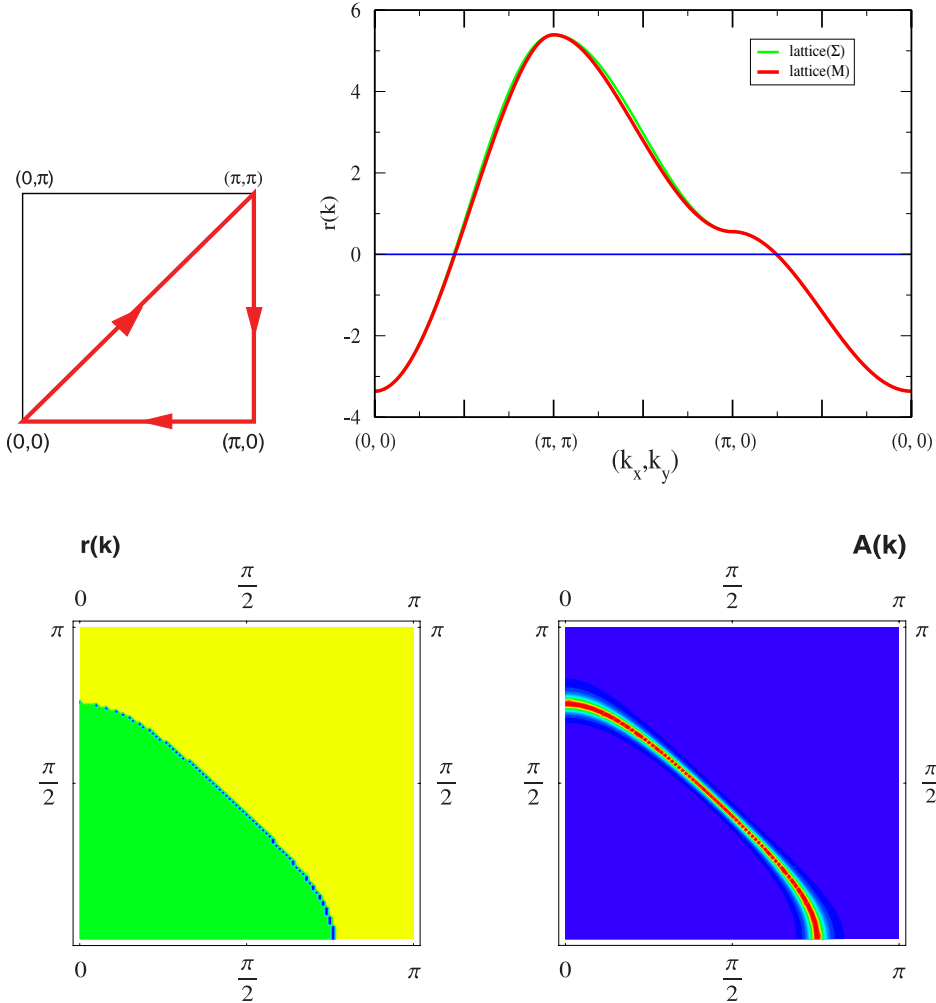
Fig. 20. Upper panel: renormalized energy $r(\mathbf{k})$ along a path in the Brillouin zone, $(k_x, k_y) = (0,0) \rightarrow (\pi, \pi) \rightarrow (\pi, 0) \rightarrow (0,0)$ in the cumulant re-construction scheme (red) and self-energy reconstruction scheme (green). Lower panels: (left) color code representation of the renormalized energy in the cumulant periodization scheme, green $(r < 0)$, blue $(r = 0)$, and yellow $(r > 0)$; (right) spectral function $A(\mathbf{k}, 0)$ in the cumulant scheme. The calculations were done for a 2D Hubbard model with $U = 8t$ for $n = 0.78$ and $T = 0$ using a CDMFT + ED approach. (For interpretation of the references to color in this figure legend, the reader is referred to the web version of this paper.)

Fermi surface we observe a line of divergences of the renormalized energy, i.e. zeros of the Green's function (red color in the upper panels of Fig. 23). We stress that the only well defined quasiparticles correspond to a vanishing $r(\mathbf{k})$ and are located along the Fermi surface. For doping levels smaller than 10% the Fermi surface is represented by a hole pocket. The pocket shrinks as we reduce the doping x and, within the present approximation, disappears for $x < 5\%$, while the line of zeros persists. In this regime the Fermi surface does not coincide with the location of the maxima of the spectral function which may have
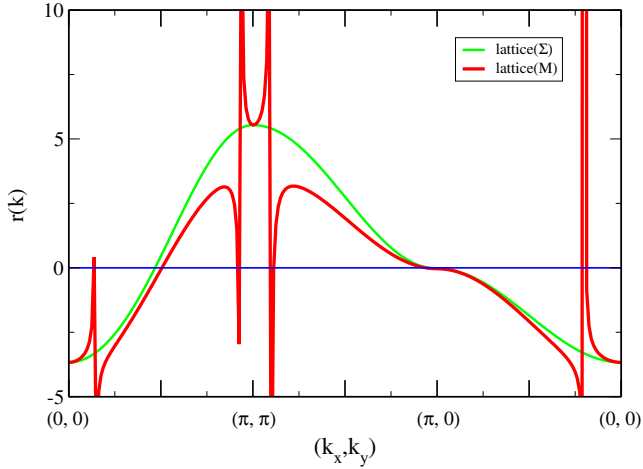
Fig. 21. Renormalized energy along a path in the Brillouin zone (same as in Fig. 20) for a filling $n = 0.78$. The other parameters are the same as in Fig. 20.
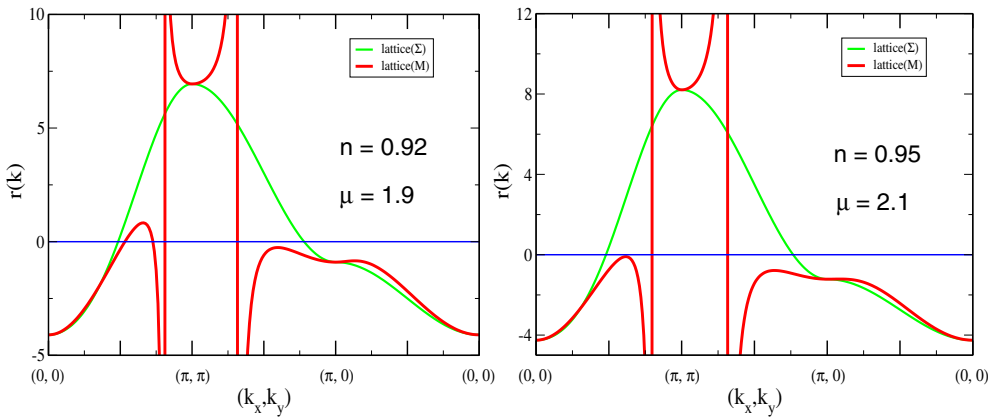

Fig. 22. Renormalized energy along a path in the Brillouin zone for a filling $n = 0.92$ (left) and $n = 0.95$ (right). The other parameters are the same as in Fig. 20.

coherent contributions coming from the quasiparticles, as well as important incoherent contributions. For example, if $n = 0.95$ (Fig. 23 lower middle panel), the entire contribution to the zero frequency spectral function is incoherent, i.e. there are no zero frequency quasiparticles. To understand the relationship between the presence of a line of zeros of the Green's function and the opening of a pseudogap at the Fermi level we calculate the frequency dependence of the spectral function for different points in momentum space. As we show in Fig. 24, the points on the Fermi surface, for example A and B in the figure, are characterized by peaks in the spectral function centered at zero frequency. However, in the proximity of the zero line (point B) the spectral weight is strongly suppressed. Therefore, the closed Fermi line that obtains at small doping *appears* in the zero frequency spectral function as an *arc* due to the presence of the zeros near the "dark side" of the Fermi
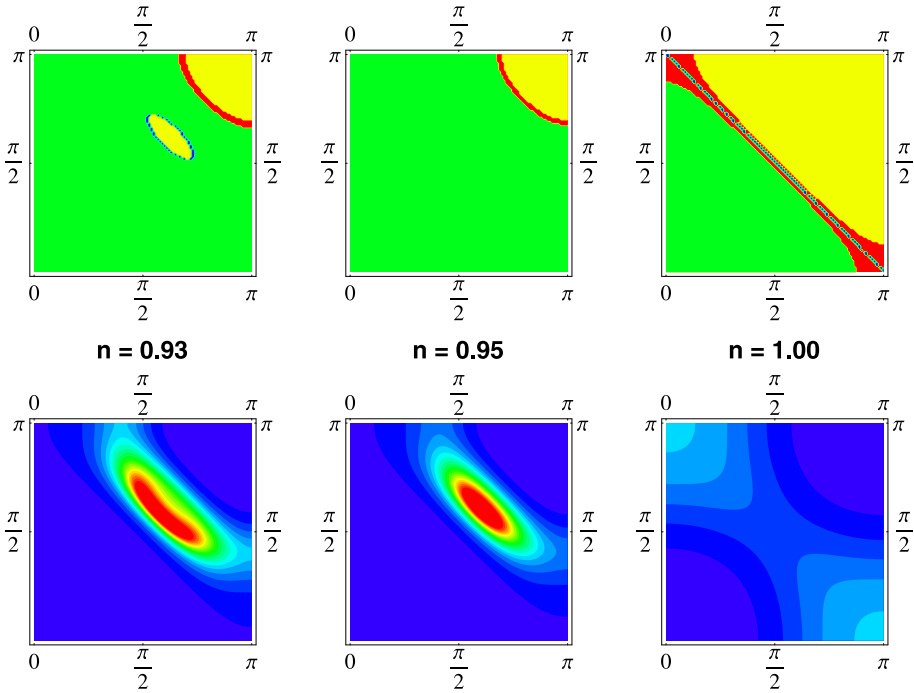
Fig. 23. Renormalized energy (upper panels) and spectral function (lower panels) for various values of filling using the short-range cumulant assumption. The color code for the upper panels is: green ($r < 0$), blue ($r = 0$), yellow ($r > 0$), and red ($|r| \rightarrow \infty$). The parameters for the Hubbard model are the same as in Fig. 20 and the scale for $A(\mathbf{k})$ is relative. (For interpretation of the references to color in this figure legend, the reader is referred to the web version of this paper.)

bubble. In addition, the proximity of the zero line determines a shift of the spectral function peak away from zero frequency for k-points that are not on the Fermi line (point C in Fig. 24). This shift is responsible for the opening of a momentum dependent pseudogap at the Fermi energy which we identify with the pseudogap seen in leading edge study of photo emission experiments. Notice that this small shift is distinct from the larger gap between the peaks above and below the Fermi level.

We may ask the question whether the lines of zeros at or near a Mott insulator can be associated with the Luttinger theorem [44] in its generalized form [45],

$$\frac{N}{V} = 2 \int_{\mathrm{Re}\, G(\mathbf{k},\omega=0)>0} \frac{\mathrm{d}^2\mathbf{k}}{(2\pi)^2}. \tag{36}$$

A change of sign for the Green's function may take place by passing through either a pole or a zero. Consequently, the generalized Luttinger theorem states that the volume enclosed by the surfaces of both poles **and zeros** yields the particle density. In principle, the existence of zeros opens the interesting possibility of having a strongly correlated system with a small Fermi surface, or no Fermi surface at all, that satisfies Luttinger theorem. However, our cluster calculations show that the theorem is not satisfied in the small doping regime ($x < 20\%$), except at half filling where extra symmetries are present (see Fig. 24, upper left panel). This violation may suggests a breakdown of the weak-coupling skeleton expansion
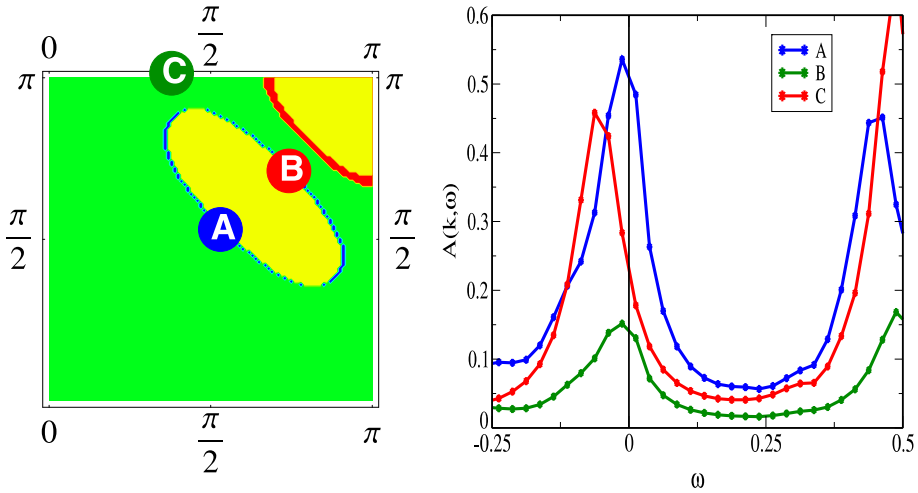
Fig. 24. Frequency dependence of the spectral function for different points in the Brillouin zone. On the Fermi surface (point A) the spectral function has a peak at $\omega = 0$, while in the pseudogap region (point C) the peak of the spectral function is shifted to negative energies. At point B the spectral weight is suppressed by the proximity of the zero line.

used in the proof of the theorem. To determine the exact shape of the surface of zeros for an arbitrary doping would require large cluster approximations that are not yet available. However, the main message of our analysis is that the zeros exist and they are closely connected to key features of Mottness that emerge from strong correlations. The last piece of evidence that we present in support of this view, is a comparison between the CDMFT results obtained for the Hubbard model using 2-site and 4-site cluster approximations shown in Figs. 25 and 26. We notice that both approximations produce the same qualitative picture. In particular they predict the existence of a line of divergences in $r(\mathbf{k})$, i.e. a line of zeros of the Green function, near the (π, π) region of the Brillouin zone. Is it significant that in the link approximation the Fermi surface is again hole-like and has a "dark side" in the proximity of the zero line, in spite of the fact that a bubble-shaped surface is prohibited by the specific k-dependence of the form $F(\mathbf{k}) = F(\cos(k_x) + \cos(k_y))$. The consistency of these two approximations is particularly evident in Fig. 25 (blue and orange lines). We stress that the lines of zeros are not a necessary consequence of the periodization scheme that we used, namely Eq. (35), but a consequence of the fact that the off-diagonal cluster self-energies are large in comparison with the diagonal components. We interpret this as a signature of the non-locality of the lattice self-energy. In particular, for the 4-site cluster we have the ratios

$$\frac{|\Sigma_{12}|}{|\Sigma_{11} - \mu|} = 2.923$$

$$\frac{|\Sigma_{13}|}{|\Sigma_{11} - \mu|} = 4.461 \tag{37}$$

$$\frac{|M_{12}|}{|M_{11}|} = 0.876$$
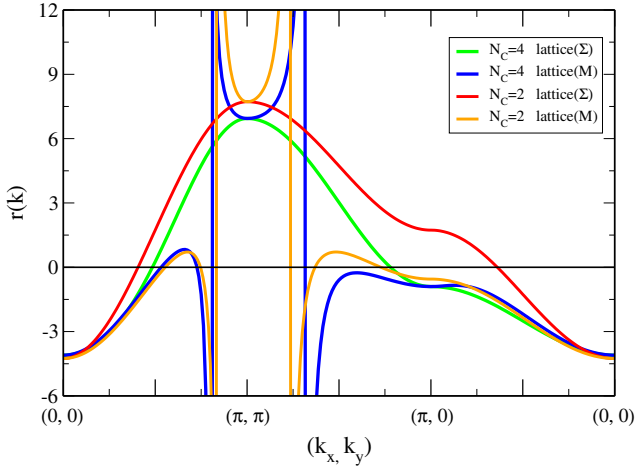
$$\frac{|M_{13}|}{|M_{11}|} = 0.626 \tag{38}$$

Fig. 25. Variation of the cumulant and self-energy solutions for the renormalized energy with the cluster size. The calculation was done for a 2D Hubbard model with $U = 8t$ and $n = 0.92$ using CDMFT + ED.
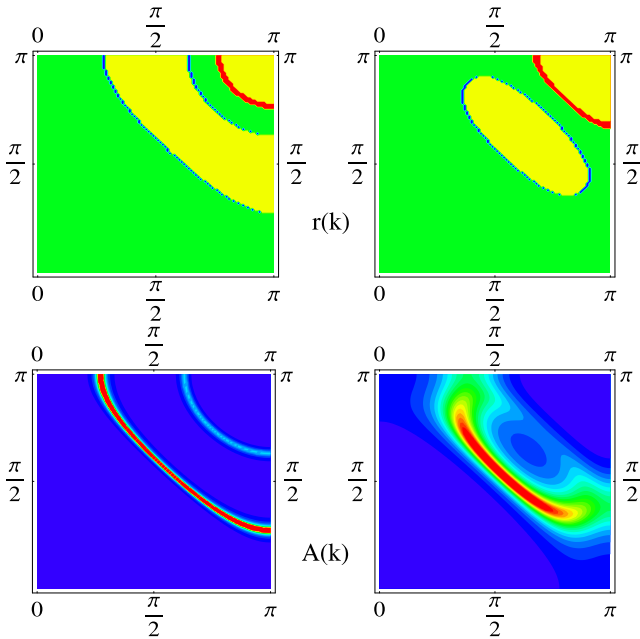

Fig. 26. Comparison between the 2-site (left panels) and 4-site (right panels) CDMFT solutions for the 2D Hubbard model with $U = 8t$. The upper panels represent the renormalized energy, while the lower panels represent the spectral function (cumulant solution).

This is in sharp contrast with the situation at large doping, for example at $n = 0.78$ where we get $|\Sigma_{12}|/|\Sigma_{11} - \mu| = 0.24$ and $|\Sigma_{13}|/|\Sigma_{11} - \mu| = 0.29$, and shows that, close to the Mott phase, any procedure based on the assumption that the self-energy is a local

quantity (or, equivalently, a smoothly varying function of momentum) is bound to fail. On the other hand, it also shows that the cumulant range at finite doping is larger than the cluster size used in the calculation, which implies that our approximation is not able to provide quantitative predictions for the shape and location of the Fermi and zero lines. Nevertheless, we believe that the rich physics uncovered by this CDMFT analysis springs from the very essence of Mottness and deserves further investigation.

5. Concluding remarks

We have shown that the cluster DMFT methodology is intimately related to the physics of strongly correlated systems. Mottness is dominated by short-range physics. From here, dynamically generated gaps, pseudogaps, broad spectral features, Fermi arcs, the breakup of the Fermi surface and other non Fermi liquid-like features emerge. Their hallmark is the existence of a surface of zeros of the one particle Green's function in the zero temperature limit. For values of the momentum corresponding to a surface of zeros the self-energy diverges, meaning that its real space Fourier transform is long-range. Therefore, the self-energy is not a quantity well suited to describe the short-range physics associated with Mottness and, consequently, any approximation that involves a short-range assumption for the self-energy is bound to fail. We identify the two-point cumulant as the best candidate for a short-range irreducible quantity that naturally captures the physics underlying Mottness. A cluster DMFT scheme based on cumulants, such as the one described in the present article, is tailor made to provide non-perturbative approximations for cumulants with a range smaller than the size of the cluster. As we have shown, even small cluster calculations open new and sometimes surprising perspectives on the behavior of highly correlated electron systems providing results that are consistent with many of the features observed experimentally in cuprate superconductors. Future large cluster calculations are expected to deliver results that can be quantitatively compared with experiments. Moreover, the large cluster calculations could answer a series of open questions. A direct determination of the range of the irreducible quantities, in particular of the cumulant, should clearly establish the possibility and the requirements for cluster approximations that are quantitatively relevant. In particular, one should be able to observe that the cumulant becomes practically negligible at distances comparable with the cluster size. With the available techniques, this is presently possible only in one dimension. Finally, the evolution of the topology of the Fermi and zero surfaces and its possible connection to an underlying critical point at finite doping in the cuprate phase diagram deserve further investigation.

References

[1] N.F. Mott, Proc. Phys. Soc. A 62 (1949) 416;
    Can. J. Phys. 34 (1956) 1356;
    Phylos. Mag. 6 (1961) 287.
[2] J. Hubbard, Proc. Roy. Soc. (London) A 281 (1964) 401.
[3] W. Metzner, D. Vollhardt, Phys. Rev. Lett. 62 (1989) 324.
[4] E. Muller-Hartmann, Z. Phys. B 74 (1989) 507.
[5] A. Georges, G. Kotliar, Phys. Rev. B 45 (1992) 6479.
[6] M. Jarrell, Phys. Rev. Lett. 69 (1992) 168.
[7] A. Georges, G. Kotliar, W. Krauth, M.J. Rozenberg, Rev. Mod. Phys. 68 (1996) 13.
[8] M.H. Hettler, A.N. Tahvildar-Zadeh, M. Jarrell, T. Pruschke, H.R. Krishnamurthy, Phys. Rev. B 58 (1998) R7475.
[9] A.I. Lichtenstein, M.I. Katsnelson, Phys. Rev. B 62 (2000) R9283.
[10] G. Kotliar, S.Y. Savrasov, G. Palsson, G. Biroli, Phys. Rev. Lett. 87 (2001) 186401.
[11] M. Potthoff, Eur. Phys. J. B 32 (2003) 429;
     Phys. Rev. Lett. 91 (2003) 206402.
[12] T. Maier, M. Jarrell, T. Pruschke, M.H. Hettler, Rev. Mod. Phys. 77 (2005) 1027.
[13] S. Moukouri, M. Jarrell, Phys. Rev. Lett. 97 (2001) 167010.
[14] T.D. Stanescu, P. Philips, Phys. Rev. B 64 (2001) 235117.
[15] O. Parcollet, G. Biroli, G. Kotliar, Phys. Rev. Lett. 92 (2004) 226402.
[16] D. Sénéchal, A.-M.S. Tremblay, Phys. Rev. Lett. 92 (2004) 126401.
[17] T. Maier, M. Jarrel, T. Pruschke, J. Keller, Eur. Phys. J. B 13 (2000) 613;
     M. Jarrel, T. Maier, M.H. Hettler, A.N. Tahvildar-Zadeh, Europhys. Lett. 56 (2001) 563.
[18] T.D. Stanescu, P. Philips, Phys. Rev. Lett. 91 (2003) 017002.
[19] B. Kyung, S.S. Kancharla, D. Sénéchal, A.-M.S. Tremblay, M. Civelli, G. Kotliar, Available from: cond-mat/0502565 (2005).
[20] M. Civelli, M. Capone, S.S. Kancharla, O. Parcollet, G. Kotliar, Phys. Rev. Lett. 95 (2005) 106402.
[21] S.S. Kancharla, M. Civelli, M. Capone, B. Kyung, D. Sénéchal, G. Kotliar, A.-M.S. Tremblay, Available from: cond-mat/0508205 (2005).
[22] Th.A. Maier, Physica B: Condensed Matter 359–361 (2005) 512.
[23] T.D. Stanescu, G. Kotliar, Available from: cond-mat/0508302 (2005).
[24] G. Biroli, G. Kotliar, Phys. Rev. B 65 (2002) 155112.
[25] D. Sénéchal, D. Perez, M. Pioro-Ladrière, Phys. Rev. Lett. 84 (2000) 522.
[26] A. Damascelli, Z.X. Shen, Z. Hussain, Rev Mod. Phys. B 75 (2003) 473.
[27] J.C. Campuzano, M.R. Norman, M. Randeria, in: K.H. Bennemann, J.B. Ketterson (Eds.), Physics of Superconductors, vol. II, 2004, pp. 167–273.
[28] T.D. Stanescu, G. Kotliar, Phys. Rev. B 70 (2004) 205112.
[29] A. Schiller, Phys. Rev. B 60 (1999) 15660.
[30] A.M. Shvaika, Phys. Rev. B 67 (2003) 75101;
     Phys. Status Solidi B 236 (2003) 368.
[31] T.D. Stanescu, P. Philips, Phys. Rev. B 69 (2004) 245104.
[32] S. Sachdev, J. Ye, Phys. Rev. Lett. 70 (1993) 3339.
[33] A.M. Sengupta, A. Georges, Phys. Rev. B 52 (1995) 10295.
[34] H. Kajueter, Ph.D. thesis, Rutgers University, 1996.
[35] Q. Si, J.L. Smith, Phys. Rev. Lett. 77 (1996) 3391;
     J.L. Smith, Q. Si, Phys. Rev B 61 (2000) 5184.
[36] R. Chitra, G. Kotliar, Phys. Rev. Lett. 84 (2000) 3678;
     Phys. Rev. B 63 (2001) 115110.
[37] W. Metzner, Phys. Rev. B 43 (1991) 8549.
[38] T.D. Stanescu, K. Haule, G. Kotliar, (unpublished).
[39] F.H.L. Essler, A. Tsvelik, Phys. Rev. Lett. 90 (2003) 126401, 1–4.
[40] F.H.L. Essler, A.M. Tsvelik, Phys. Rev. B 65 (2002) 115117, 1–13.
[41] R.M. Konik, T.M. Rice, A.M. Tsvelik, Available from: cond-mat/0511268.
[42] T.D. Stanescu, P. Philips, T.-P. Choy, Available from: cond-mat/0602280.

[43] C. Berthod, T. Giamarchi, S. Biermann, A. Georges, Available from: cond-mat/0602304.
[44] J.M. Luttinger, Phys. Rev. 119 (1960) 1153–1163.
[45] I. Dzyaloshinskii, Phys. Rev. B 68 (2003) 085113.